Master's Thesis
Theoretical Physics

Topological superconductivity in regular and random lattices

Isac Sahlberg

2018

Supervisor: Dr. Teemu Ojanen

Examiners: Dr. Teemu Ojanen
Prof. Kai Nordlund

UNIVERSITY OF HELSINKI
Department of Physics

P.O. Box 64 (Gustaf Hällströmin katu 2)
00014 Helsingin yliopisto

HELSINGIN YLIOPISTO — HELSINGFORS UNIVERSITET — UNIVERSITY OF HELSINKI

Tiedekunta — Fakultet — Faculty	Laitos — Institution — Department
Faculty of Science	Department of Physics

Tekijä — Författare — Author
Isac Sahlberg

Työn nimi — Arbetets titel — Title

Topological superconductivity in regular and random lattices

Oppiaine — Läroämne — Subject
Theoretical Physics

Työn laji — Arbetets art — Level	Aika — Datum — Month and year	Sivumäärä — Sidoantal — Number of pages
Master's Thesis	2018	64 pages

Tiivistelmä — Referat — Abstract

In this thesis, we examine a fairly novel area of physics that concerns topological materials, and in particular, topological superconductivity. A goal in the research of topological materials is realizing applications in quantum computing, which could be aided by the emergent quasiparticles that exhibit non-Abelian exchange statistics. These are called Majorana bound states, and they are elusive quasiparticles predicted to be found on the boundary of topological superconductors.

We first study a one-dimensional chain of potential impurities placed on the surface of a two-dimensional p-wave superconductor. As is usually the case, such chains are composed of perfect lattice structures, which is very challenging to achieve in any laboratory setting. Nevertheless, they serve as a good example of systems where an analytical solution can be well established. We investigate the model without employing any deep-dilute approximation, which gives us an accurate description even far away from the gap center. This is done by formulating the problem as a non-linear eigenvalue equation, which complicates it significantly, but also extends the region of applicability of our theory. We use reciprocal space calculations of two topological invariants to obtain the topological phase diagram of the system. The model is shown to host topological quasiparticle excitations at the ends of the chain, with multiple distinct topological phases. The near-perfect localization of the excitations makes them good candidates for probing Majorana bound states in experimental setups.

We then move on to study topological superconductivity in random lattices, as opposed to regular structures which assume arbitrary precision. We frame our work starting with the mathematics of random numbers. Our work is thus in stark contrast with previous studies on topological materials that start off with a perfect lattice structure, and investigate some degree of disorder as perturbations to the regular lattice case. Our work establishes a first-ever realistic candidate for realizing topological superconductivity in an amorphous material. This could enable a novel approach to creating topological materials, and drastically aid in the development of fault-tolerant quantum computing.

Avainsanat — Nyckelord — Keywords
Topological superconductivity, Majorana, non-linear eigenvalue problem, random lattices

Säilytyspaikka — Förvaringsställe — Where deposited

Muita tietoja — övriga uppgifter — Additional information

Contents

1. Introduction

Topology is the branch of mathematics concerned with sets or *spaces* where some properties stay invariant under continuous deformations of those spaces. The process of stretching and bending a material (more precisely, deforming a mathematical space) is a *continuous* transformation, while tearing or puncturing is not. Topological materials exhibit quantum phases of matter which in some sense have non-trivial topology. The phases of matter hosted in this kind of matter have then an intrinsic robustness, meaning that any continuous transformation on it (or a *small* perturbation) will not get rid of the underlying topology.

The robustness against changes in the topological phase makes these topological materials interesting for applications in quantum computing, where the biggest issue is sustaining the interplay between phases of matter which is so easily lost due to quantum decoherence.[1] Of course, you could imagine setting up a superposition of quantum states, such as two wave functions of an electron, in a completely *closed* system, and it would remain in that superposition forever — but as soon as you want this system to communicate with the outside world, you inevitably introduce a means for it to break apart, and your information will likely be lost. Studying topological matter is not only interesting from the point of view of fundamental research, it could offer major breakthroughs in quantum information processing. Indeed, the study of topological phases has attained much attention during the last

[1] By this we mean the loss of information into the environment, which is difficult to prevent due to the overwhelming number of constituents in a macroscopic system.

few decades. The 2016 Nobel Prize in Physics was awarded to Thouless, Haldane and Kosterlitz for their contributions to the study of topological phases and phase transitions.

Above we mentioned that topological spaces have certain properties that stay invariant under continuous transformations. The character of these features is captured by what are known as topological invariants. They are usually given by a mathematical formula which only takes on integer values – these integers only change when moving between topologically distinct spaces, and in particular, they *cannot* change under continuous transformations, since in that case we remain in a topologically equivalent space.

One can very simply make topology appear in everyday materials by creating what is known as a *Möbius* strip. The way to construct one is by taking a ribbon of paper and connecting the two loose ends, but with carefully twisting the different ends of the ribbon such that the twisting makes up half a rotation. Now there is in fact no way to get to a "normal" band by only performing continuous manipulations on the strip. Instead, one has to *cut* it – but this is not a continuous transformation – so the two strips are topologically distinct.[2]

In the remainder of this thesis, we will not talk about topological spaces, but rather about topological phases of matter. The difference is subtle; the topology of the phases is rooted in the quantum-mechanical operators that live in the corresponding Hilbert spaces. So at the deepest level, the topology lives in the mathematical spaces given by the physical theory of quantum mechanics. But, as we will see, topologically non-trivial phases can exhibit physical realizations that free us up to think about the topology in much easier terms.

An important concept that we will encounter frequently in this thesis is the

[2]By instead twisting the ends any number of times before connecting them, you can reach multiple configurations that are *all* topologically distinct. In the language of the above paragraph, this system is described by an *integer* topological invariant.

energy gap. It is the energy difference separating the excited states from the ground state. Thus the energy gap is the minimum energy that an electron needs to move to an unoccupied, higher-energy state. The highest energy of the occupied states is called the Fermi energy. Throughout this thesis, we have set the Fermi energy to zero, and we can thus simply talk about energies when we mean energy differences to the ground state. Now, it is a well-known fact that topologically inequivalent phases are described by Hamiltonians that cannot be continuously transformed to each other without closing the gap.[3] We will encounter topological phase diagrams where between all different phases there is a boundary with zero energy in the corresponding spectrum diagram. In addition to having gap closings at all boundaries between different topological phases, the magnitude of the gap serves as a measure of the robustness of the topological phase.

Topological phases have recently been shown to exist in systems that lack a regular lattice structure [2]. The prospect of topological materials being realized in *glassy* systems is exciting, because it could open up a whole new approach to bringing about applications for topological phases. There is a large difference between assembling impurities in perfect lattice structures and simply gathering enough impurities in a certain system. Indeed, as we will see in subsequent chapters, our model of amorphous topological superconductivity supports a topological phase simply above a *critical impurity density*. As the need for precision when constructing topological matter decreases, the change in the engineering involved may at best lead to a completely new industry of producing materials with topological quantum properties.

In this thesis, we investigate two highly contrasting models of topological superconductivity. The first concerns one-dimensional (1D) chains of scalar impurities

[3]Technically, the gap does not have to close in a topological phase transition, provided that during the process, the symmetry of the system *changes*. [1] However, these cases will not concern us in this thesis.

deposited on a two-dimensional (2D) p-wave superconductor, and the second concerns 2D magnetic lattices which completely lack any spatial order, derived from a model known to host a rich structure of topological phases. The structure of the thesis is as follows: After briefly introducing the role of topology in physics, in Sec. 1.1, we discuss the importance of quantum-mechanical effects in condensed matter physics and their role in quantum information processing. In Ch. 2, we concern ourselves with superconductivity and its connection to topological superconductivity. In Sec. 2.1, we give a brief introduction to superconductors within the BCS theory, tying it to topological superconductivity in Sec. 2.2. We present a classic example of a toy model of topological superconductivity, which illustrates non-trivial topological properties in condensed matter systems without too many complications.

In Ch. 3, we begin with the system of one-dimensional chains of scalar impurities deposited on a two-dimensional spinless p-wave superconductor. We derive the energy spectrum of the system by first expressing the problem as a non-linear eigenvalue equation and going over to reciprocal space in Sec. 3.1. In Sec. 3.2, we investigate the topological properties of the system, and present two relevant topological invariants, and in Sec. 3.3, we generalize the results to a spinful superconductor. In Sec. 3.4, we present the energy gap and topological phase diagrams, and justify a physical interpretation of the topological invariants in Sec. 3.4.1.

In Ch. 4, we present our work on topological superconductivity in two-dimensional random lattices, beginning with the underlying model in Sec. 4.1. In Sec. 4.2, we concern ourselves with the topology of this random system, presenting an applicable topological invariant in Subsec. 4.2.1. In Subsec. 4.2.2, we expand on the connection between energy gaps and robustness of the topological phases, and argue why the true energy gap of this system is not applicable in a direct way, and show how the mobility gap actually signifies the stability of the phases. We present the

topological phase diagram of the system in Sec. 4.3, and show the emergence of edge modes in finite 2D lattices. We end the chapter with Sec. 4.4, where we discuss a possible explanation for the emergence of non-trivial topological phases in systems lacking spatial order.

In the final chapter, we give a summary of the presented works and discuss some future applications. In addition to these chapters, we include three appendices in this thesis. Important technicalities are moved to the appendices; in Appendix A, we derive the non-linear eigenvalue problem of Ch. 3, in Appendix B we solve the related energy spectrum, and in Appendix C we present the Hamiltonian of the underlying superconducting model employed in Ch. 4 in more detail.

Ch. 3, which focuses on the 1D chain of scalar impurities, is based on research conducted by the author and collaborators, and is contained in Ref. [3]. Also, as of this writing, the authors have submitted a preprint [4] of a work on the topology in amorphous lattice systems, encapsulating the work of Ch. 4 on random lattices presented in this thesis.

1.1 Quantum computing

The theories describing essentially all static and dynamic properties of solids, liquids and gases at long wavelengths[4] were formulated by the end of the nineteenth century. It was the theories of quantum mechanics that led physicists to a more complicated, microscopic investigation of condensed matter. In his famous 1972 paper titled "More is different" [5], P. W. Anderson describes why it is crucial that we give importance to research on all scales including solid state or many-body physics. It is not enough to just investigate physics on the most fundamental level as in elementary particle physics, since even perfect knowledge in that area does not lead

[4] As is customary in condensed matter physics, by this we mean long compared to atomic length scales.

us to know how a macroscopic number of particles interact with each other. In essence, the interplay between a large number of particles gives rise to entirely new physics. Condensed matter physics is the study of just these kinds of new phenomena that do not exist on the atomic scale; it is the study of different many-body states of matter.

In stark contrast to classical physics, because we cannot keep track of particles in quantum mechanics, there is no way to fundamentally define distinguishability. Instead of always describing each particle separately, many particles are then described by common *wave vectors* (or wave functions). When we talk about exchange statistics, we mean the change to the common wave vector that occurs when the positions of two indistinguishable particles are swapped. Now, in three dimensions, this indistinguishability leads to only *two* types of particles: bosons and fermions. In two dimensions, however, the exchange of two particles can depend on the particular path traversed by the particles. In such cases, the particles are called *anyons*. Even though they were first studied as theoretical curiosities, anyons can be encountered in effectively two-dimensional physical systems. [6]

Majorana bound states (MBSs) are quasiparticle excitations that have exotic properties, most notably their non-Abelian braiding statistics. We will encounter MBSs later in this thesis. Topological quantum computers hold considerable promise, since the quantum information is embedded non-locally – in a way that is intrinsically decoherence-free. Topological quantum computing relies on the braiding of anyons in a 2D lattice; the non-Abelian exchange statistics of the MBSs leads to protected operations on quantum information. [7, 8]

Quantum computing caught the interest of the physics community in the early 1980s. Richard Feynman was among the first to introduce the principles for why quantum computers could theoretically be superior to conventional computers. [9] In the recent decades, there has been active research in the area of quantum comput-

ing, which exploits the quantum-mechanical properties of small systems to perform calculations. Quantum computing has the potential to revolutionize the modern world, which is increasingly filled with electronic devices. It is, however, likely to first impact research and industry, with calculations that require much more resources, due to the immense size of current quantum computers and the difficulty of scaling them down.

Recently, quantum computers have begun to overtake conventional computers in certain computations, albeit in very restricted environments. [10] Quantum computers are based on so-called qubits, which differ drastically from the classical bits that can only have one of two values – 0 or 1. Currently, decoherence poses the biggest obstacle in the development of useful quantum computing systems. One elegant way to circumvent this problem is the use of topological phases, and in particular, the quasiparticle excitations that are hosted by these phases. An important detail to appreciate about these excitations is that they are protected by the topological phases, and thus carry an inherent robustness towards the loss of information. The non-Abelian braiding statistics of the quasiparticle excitations allow for topologically protected qubits. The encoding of the quasiparticle states are non-local, which protects a topological quantum computer from errors due to local perturbations. [11, 12] The fact that they are localized at the boundary of the material is also useful; as we will see in Subsec. 3.4.1, our model of the 1D chain of impurities hosts essentially perfectly localized pairs of MBSs at the ends of the chain. This is considerably helpful when it comes probing and manipulation of such quasiparticle excitations.

2. Theory

In this chapter, we will concern ourselves with simple models of superconductivity and topological superconductivity. In Sec. 2.1, we briefly discuss superconductivity as a phenomenon, and introduce the BCS theory of superconductivity and the Bogoliubov-de Gennes formalism. In Sec. 2.2, we move on to present a toy model of topological superconductivity proposed by Kitaev, and tie it to knowledge gained in the preceding section.

2.1 BCS theory of superconductivity

We begin with the phenomenon of superconductivity itself. It refers to the completely new form of conductivity where the aptly named superconductor has vanishing electrical resistance at very low temperatures. Just over a century ago, in 1911, K. Onnes discovered [13] that when various metals were cooled below a *critical temperature* T_c which depends on the cooled material, they would lose their electrical resistance completely. However, a strong applied magnetic field destroyed the perfect conductivity. But it was not just perfect conductivity that was discovered: Meissner and Ochsenfeld discovered [14] that superconductors, in the presence of an applied magnetic field, completely *expelled* all interior magnetic fields, and did so as they were cooled through their critical temperature.[1] Superconductivity was thus demonstrated to be more than just perfect conductivity, which would prevent

[1] This phenomenon is now known as the Meissner effect.

the magnetic flux through the surface of the conductor from changing, i.e. instead trapping the magnetic flux in. [15] Now, at first superconductors seem to be the perfect materials for use in transmission lines and electronic devices, since they would get rid of any heat losses. The caveat to this is that superconductors require very low temperatures, and even the so-called high-temperature superconductors (HTS) require temperatures far below room temperature. An obvious advantage of the HTSs is that no liquid helium is required to cool the material, but on the other hand thermal fluctuations are much more prominent, leading to resistance. A microscopic theory for the mechanism behind superconductivity at high temperatures remains elusive. To date, the highest T_c observed is 203 K in hydrogen sulfide. [16]

Now we will briefly introduce the BCS theory of superconductivity by Bardeen, Cooper and Schrieffer. [17, 18] Nearly 50 years after the intial discovery of the phenomenon, the 1957 theory by BCS was the first theoretical microscopic description of superconductivity. It accounts for the properties of conventional superconductors with remarkable success. (It does not completely explain the properties of high-temperature superconductivity, and there is ongoing research for a suitable, modified theory.) The starting point for the superconducting state is a non-interacting electron gas. With an attractive interaction between pairs of electrons, quasiparticle excitations called Cooper pairs form near the Fermi level. They are composite bosons of zero momentum and zero spin – electrons of opposite momenta and spin are coupled. With a phonon-mediated interaction coupling these quasiparticles, we can write down the BCS Hamiltonian as

$$H = \sum_{\mathbf{k}\sigma} \xi_{\mathbf{k}} c^\dagger_{\mathbf{k}\sigma} c_{\mathbf{k}\sigma} + \sum_{\mathbf{k}\mathbf{k}'} V_{\mathbf{k}\mathbf{k}'} c^\dagger_{\mathbf{k}\uparrow} c^\dagger_{-\mathbf{k},\downarrow} c_{-\mathbf{k}',\downarrow} c_{\mathbf{k}'\uparrow}, \tag{2.1}$$

where $\xi_{\mathbf{k}} = k^2/2m - \mu$ stands for the single-particle energy relative to the Fermi energy, and the latter sum is our interaction term, with $V_{\mathbf{k}\mathbf{k}'}$ specifying the nature of the interaction. The $c^\dagger$,c are the creation and annihilation operators for an electron

of momentum[2] $\mathbf{k}$ and spin σ. It is an effective Hamiltonian written in the language of second quantization that describes the interaction between the Cooper pairs near the Fermi level. As such, the interaction is non-zero only for $|\xi_{\mathbf{k}}|, |\xi_{\mathbf{k}'}| < \omega_D$, where ω_D is the Debye frequency. [19]

The assumption by BCS is that in the superconducting state, the electrons condense into Cooper pairs, so we have a non-zero expectation value for the operator $c^\dagger_{\mathbf{k}\uparrow}c^\dagger_{-\mathbf{k},\downarrow}$. Additionally, well below the critical temperature T_c, the fluctuations around this mean value are small. Then, the so-called *mean-field* approximation relies on the following identity:

$$0 \approx (X - \langle X\rangle)(Y - \langle Y\rangle) = XY - \langle X\rangle Y - X\langle Y\rangle - \langle X\rangle\langle Y\rangle, \tag{2.2}$$

which is valid if deviations from the mean value of the operators X, Y are small[3]; the error made in the approximation is of second order in the deviations. Applying this approximation on the operators $c^\dagger_{\mathbf{k}\uparrow}c^\dagger_{-\mathbf{k},\downarrow}$ and $c_{-\mathbf{k}',\downarrow}c_{\mathbf{k}'\uparrow}$, we obtain the mean-field BCS Hamiltonian

$$H = \sum_{\mathbf{k}\sigma} \xi_{\mathbf{k}} c^\dagger_{\mathbf{k}\sigma}c_{\mathbf{k}\sigma} + \sum_{\mathbf{k}\mathbf{k}'} V_{\mathbf{k}\mathbf{k}'} \left(\langle c^\dagger_{\mathbf{k}\uparrow}c^\dagger_{-\mathbf{k},\downarrow}\rangle c_{-\mathbf{k}',\downarrow}c_{\mathbf{k}'\uparrow} + c^\dagger_{\mathbf{k}\uparrow}c^\dagger_{-\mathbf{k},\downarrow}\langle c_{-\mathbf{k}',\downarrow}c_{\mathbf{k}'\uparrow}\rangle \right) + \text{const.} \tag{2.3}$$

Now, ignoring the additive constant (which only amounts to shifting the energy eigenvalues) and defining $\Delta_{\mathbf{k}} = -\sum_{\mathbf{k}'} V_{\mathbf{k}\mathbf{k}'}\langle c_{-\mathbf{k}',\downarrow}c_{\mathbf{k}'\uparrow}\rangle$, we can write our Hamiltonian in the form

$$H = \sum_{\mathbf{k}\sigma} \xi_{\mathbf{k}} c^\dagger_{\mathbf{k}\sigma}c_{\mathbf{k}\sigma} + \sum_{\mathbf{k}} \Delta_{\mathbf{k}} c^\dagger_{\mathbf{k}\uparrow}c^\dagger_{-\mathbf{k},\downarrow} + \sum_{\mathbf{k}} \Delta^*_{\mathbf{k}} c_{-\mathbf{k},\downarrow}c_{\mathbf{k}\uparrow} + \text{const.} \tag{2.4}$$

$$= \sum_{\mathbf{k}\sigma} \xi_{\mathbf{k}} c^\dagger_{\mathbf{k}\sigma}c_{\mathbf{k}\sigma} + \sum_{\mathbf{k}} \left(\Delta_{\mathbf{k}} c^\dagger_{\mathbf{k}\uparrow}c^\dagger_{-\mathbf{k},\downarrow} + \text{h.c.} \right). \tag{2.5}$$

This Hamiltonian describes a non-interacting system, since it is bilinear in the creation and annihilation operators $c, c^\dagger$. These are somewhat unusual terms, but

[2] We will set $\hbar = 1$ throughout this thesis, rendering momentum and wave vector the same quantity.

[3] meaning that the difference between acting with an operator on whatever objects we are considering, compared to just multiplying by the mean value of that operator, is small.

including only quadratic terms in the operators $c, c^\dagger$, the Hamiltonian should now be readily solvable. Let us write it in the form

$$H = \frac{1}{2}\sum_{\mathbf{k}} \mathbf{A}_{\mathbf{k}}^\dagger \mathbf{H}_{\mathbf{k}} \mathbf{A}_{\mathbf{k}} + \text{const.}, \tag{2.6}$$

where

$$\mathbf{A}_{\mathbf{k}} = \begin{pmatrix} c_{\mathbf{k}\uparrow} \\ c_{-\mathbf{k}\downarrow}^\dagger \end{pmatrix}, \qquad \mathbf{H}_{\mathbf{k}} = \begin{pmatrix} \xi_{\mathbf{k}} & -\Delta_{\mathbf{k}} \\ -\Delta_{\mathbf{k}}^* & -\xi_{\mathbf{k}} \end{pmatrix}. \tag{2.7}$$

The matrix $\mathbf{H}_{\mathbf{k}}$ is called the BdG Hamiltonian, and possesses so-called particle-hole symmetry (PHS). What this means is that all energies are found in pairs $\pm E$. Mathematically, particle-hole symmetry means that there exists an operator $\mathcal{C}$ s.t. $\mathcal{C}^{-1}\mathcal{H}\mathcal{C} = -\mathcal{H}^*$. In our case, this operator is given by $\mathcal{C} = \tau_y \mathcal{K}$, where $\mathcal{K}$ is the complex conjugate operator, which acts on each complex number by flipping the sign of its imaginary part. Note that we can think of the Nambu spinors $\mathbf{A}_{\mathbf{k}}$ that the BdG Hamiltonian acts on as being composed of annihilation operators for electrons *and* their corresponding holes – we have now doubled the degrees of freedom of the system. As such, the PHS follows by construction.

Next, we diagonalize the Hamiltonian using what is called a Bogoliubov transformation: We define new fermionic operators as linear combinations of the original operators:

$$\begin{pmatrix} \tilde{c}_{\mathbf{k}\uparrow} \\ \tilde{c}_{-\mathbf{k},\downarrow}^\dagger \end{pmatrix} = \begin{pmatrix} a_{\mathbf{k}} & b_{\mathbf{k}} \\ -b_{\mathbf{k}}^* & a_{\mathbf{k}}^* \end{pmatrix} \begin{pmatrix} c_{\mathbf{k}\uparrow} \\ c_{-\mathbf{k},\downarrow}^\dagger \end{pmatrix} \tag{2.8}$$

Requiring that this transformation be unitary, and that the operators $\tilde{c}_{\mathbf{k},\sigma}$ satisfy fermionic anticommutation relations, we obtain constraints on the coefficients $a_{\mathbf{k}}, b_{\mathbf{k}}$. We forego the tedious algebra, and just state that we end up with the diagonalized Hamiltonian

$$H = \sum_{\mathbf{k}} E_{\mathbf{k}} \left(\tilde{c}_{\mathbf{k},\uparrow}^\dagger \tilde{c}_{\mathbf{k},\uparrow} + \tilde{c}_{-\mathbf{k},\downarrow}^\dagger \tilde{c}_{-\mathbf{k},\downarrow} \right) \tag{2.9}$$

$$= \sum_{\mathbf{k}\sigma} E_{\mathbf{k}} \tilde{c}_{\mathbf{k},\sigma}^\dagger \tilde{c}_{\mathbf{k},\sigma} \tag{2.10}$$

where $E_{\mathbf{k}} = \sqrt{\xi_{\mathbf{k}}^2 + |\Delta_{\mathbf{k}}|^2}$. The $\tilde{c}_{\mathbf{k},\sigma}$ describe fermionic elementary quasiparticle excitations, sometimes called *Bogoliubons*.

It is instructive to first consider the normal, non-superconducting metal, corresponding to the case $\Delta_{\mathbf{k}} \to 0$. We then have for the above dispersion $E_{\mathbf{k}} = |\xi_{\mathbf{k}}|$, i.e. it any fermionic excitations have positive energy except at the Fermi level $\xi_{\mathbf{k}}$. If we "turn on" a non-zero $\Delta_{\mathbf{k}}$, i.e. consider a superconductive metal, we have opened up an energy gap $|\Delta_{k_F}|$,[4] the "superconducting gap", a non-zero minimum energy for the fermion excitations. Since the operators $\tilde{c}$ are superpositions of the operators $c, c^\dagger$, the quasiparticle excitations can be thought of as particle-hole superpositions. The energy eigenvalues $E_{\mathbf{k}}$ decrease with increasing $|\mathbf{k}|$ until the Fermi momentum k_F (where the minimum value Δ is attained) and increases after that. This gapped spectrum is ultimately responsible for the superconductivity. The gap Δ is almost constant in the limit $T \to 0$, and only when a significant amount of Bogoliubons are excited does it start to vary. [15] It decreases with increasing temperature, and as mentioned previously, the gap vanishes completely as the temperature reaches the critical temperature T_c.

2.2 Toy model of topological superconductivity

In this section we briefly tie the above theory of superconductivity to topological superconductivity. It is perhaps most instructive to take a look at the toy model proposed by Kitaev in 2001. [20] We note that there are no known candidates which could be used to construct such a toy model, but it remains useful due to its relative simplicity. [21] We will even use some of the tools introduced in the previous chapter to analyze this model. We start out with the second-quantized Hamiltonian

$$H = \sum_j \left[-t(c_j^\dagger c_{j+1} + c_{j+1}^\dagger c_j) - \mu c_j^\dagger c_j + \Delta(c_{j+1}^\dagger c_j^\dagger + c_j c_{j+1}) \right], \tag{2.11}$$

[4] The k_F label comes from recognizing that $\xi_{\mathbf{k}}^2$ is smallest at the Fermi surface.

which describes a 1D lattice chains with N lattice points. The operators a_j,$a_j^\dagger$ are annihilation and creation operators at the lattice site j, and the sum runs over all lattice points,[5] $\sum_j = \sum_{j=1}^{N}$. The first term is a simple hopping term, while the last term denotes a superconducting pairing term (Δ is the superconducting gap). Now, Δ remains a real parameter in this analysis, but the results derived here are also valid for the complex Δ case.[6] We assume that $a_{j+N} = a_j$, i.e. that the system obeys periodic boundary conditions. This is equivalent to inspecting an infinite chain. Since we now have a discrete translational symmetry in the chain, we can apply a lattice Fourier transform, defined through the relations[7]

$$c_k = \frac{1}{\sqrt{N}} \sum_j c_j e^{ilkj} \tag{2.12}$$

$$c_j = \frac{1}{\sqrt{N}} \sum_k c_k e^{-ilkj}, \tag{2.13}$$

where $l = N/L$ is the lattice constant, and L is the length of the chain. The momenta k lie within $lk \in \left\{-\pi + \frac{2\pi}{N}, -\pi + \frac{4\pi}{N}, \ldots, \pi\right\}$. A straightforward transformation into reciprocal space brings our Hamiltonian (2.11) in the form

$$H = \sum_k \left[-(2t\cos kl + \mu)c_k^\dagger c_k + \Delta e^{ikl}(c_k^\dagger c_{-k}^\dagger + c_k c_{-k})\right]. \tag{2.14}$$

The original creation and annihilation operators c_j of the chain, being fermionic operators, obey the usual anticommutation relations $\{c_j, c_{j'}^\dagger\} = \delta_{jj'}$; $\{c_j, c_{j'}\} = \{c_j^\dagger, c_{j'}^\dagger\} = 0$. From this we can easily show that identical anticommutations hold for our reciprocal-space operators $c_k, c_k^\dagger$. We would now like to massage this expression

[5] This is actually not quite true; the sum depends on the boundary conditions at hand. We will take into account the slight difference in the case of open boundary conditions below.

[6] The complex phase can actually be neatly hidden in the operators introduced below – see the original paper by Kitaev [20] – but our approach differs from it slightly, so we will simply state that the results remain the same.

[7] It is customary to place additional tildes or other symbols above the Fourier transformed quantities, but we will forego that here with no risk of confusion – they will simply have momenta k as indices.

further into a more useful form. Following the strategy laid out in the previous section, and by employing the above anticommutation relations, we can write the Hamiltonian in the form

$$H = \frac{1}{2}\sum_k \Psi_k^\dagger H_{\mathrm{BdG},k}\Psi_k + \text{const.}, \tag{2.15}$$

where we have introduced the Nambu spinor $\Psi_k = (c, c_{-k}^\dagger)^T$ (cf. Eq. (2.7)). In this case, the BdG Hamiltonian is

$$H_{\mathrm{BdG,k}} = \begin{pmatrix} -(2t\cos kl + \mu) & 2i\Delta \sin kl \\ -2i\Delta \sin kl & 2t\cos kl + \mu \end{pmatrix}. \tag{2.16}$$

As usual, we ignore the constant shift to the energy spectrum, and can focus entirely on $H_{\mathrm{BdG,k}}$. By noticing that it can be written using two Pauli matrices: $H_{\mathrm{BdG,k}} = A_k\sigma_y + B_k\sigma_z$, we can employ the following useful trick: By squaring the $H_{\mathrm{BdG,k}}$, we end up with a matrix proportional to unity, $H_{\mathrm{BdG,k}}^2 = A_k^2 + B_k^2$, so we can immediately write down the energy spectrum as

$$E_k = \pm\frac{1}{2}\sqrt{(2t\cos kl + \mu)^2 + 4\Delta^2 \sin^2 kl}. \tag{2.17}$$

This expression looks similar to the one obtained for the conventional superconductor in Sec. 2.1 – we can either have or not have a gapped spectrum for the given parameter values. There is a critical point separating the two gapped superconducting phases: if $\mu = -2t$, the gap closes at $k = 0$. But in this case, as we will see shortly, this gap closing separates two topologically distinct phases.

Let us define a new set of operators γ_j, called the Majorana operators, which will let us discern the different topological phases more clearly.

$$\begin{aligned} \gamma_{2j-1} &= c_j^\dagger + c_j \\ \gamma_{2j} &= i(c_j^\dagger - c_j) \end{aligned} \tag{2.18}$$

Note that these are all Hermitian operators, $\gamma_j^\dagger = \gamma_j$, i.e. they correspond to particles which are their own antiparticles. We will now instead assume open boundary

conditions. Then, using this transformation on the operators c_j, the Hamiltonian (2.11) takes the form

$$H = \frac{i}{2}\sum_j \left[(\Delta + t)\gamma_{2j}\gamma_{2j+1} + (\Delta - t)\gamma_{2j-1}\gamma_{2j+2} - \mu\gamma_{2j-1}\gamma_{2j}\right]. \tag{2.19}$$

Next, we are going to look at two limiting cases, which turn out to be topologically inequivalent. First, we set $t = \Delta = 0$, which gives

$$H = -\frac{i}{2}\sum_{j=1}^{N} \mu\gamma_{2j-1}\gamma_{2j}. \tag{2.20}$$

Here we have a coupling only between pairs of Majorana operators for each lattice site as defined in the original setup. If we instead set $\mu = 0$ and $\Delta = t$, the Hamiltonian becomes

$$H = i\sum_{j=1}^{N-1} t\gamma_{2j}\gamma_{2j+1}. \tag{2.21}$$

Since the labels $2j-1, 2j$ on the Majorana operators correspond to the lattice site j in our chain, this Hamiltonian couples Majorana operators from different lattice sites. Despite the conventional notation, the terms including t and Δ were in this case summed only up to $N-1$ due to open boundary conditions, and we have made that distinction explicit here.

Now, two Majorana operators, γ_1 and γ_{2N}, are left out of the Hamiltonian completely – they are unpaired. We thus see the emergence of two unpaired Majorana fermions at the ends of the chain. This quasiparticle is, in particular, highly delocalized. Inverting the set of equations (2.18), we know how to create a perfectly suitable fermionic operator out of these two Majorana operators: $c_M = (\gamma_1 + i\gamma_{2N})/2$, which satisfies the anticommutation relations along all the other operators c_j. Since these operators are absent from the Hamiltonian (2.21), a state corresponding to c_M does not change the energy of the system. Thus the ground state is two-fold degenerate, since such a *zero mode* is either present or missing.

The critical point mentioned above separates these two cases, and indeed these Majorana modes persist unless the system crosses a critical point, during which the

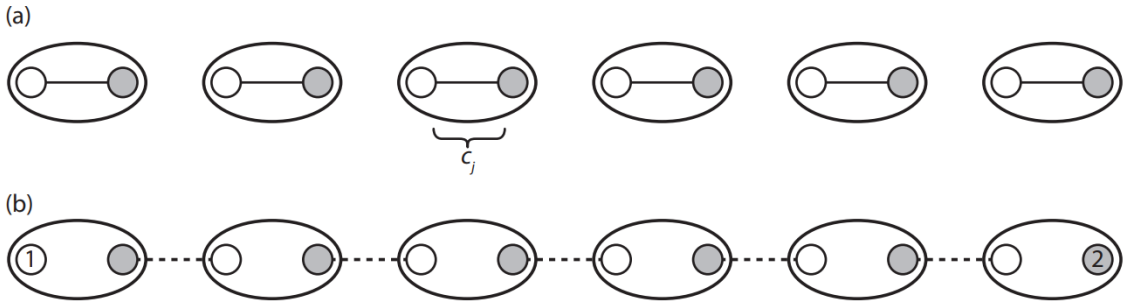

Figure 2.1: Illustration of the lattice chain for the case N=6. The fermionic operators c_j correspond to two Majorana operators $\gamma_{2j-1}, \gamma_{2j}$. (a) The parameters chosen are $\Delta = t = 0$, corresponding to the trivial phase. The couplings between the Majorana operators are all local to the lattice site (indicated by solid lines). (b) In this case $\mu = 0$ and $\Delta = t$, corresponding to the non-trivial phase. Here, the couplings are between neighboring lattice sites (dashed lines), leaving two unpaired operators at the ends of the chain. Figure taken from Ref. [21].

bulk gap is closed. The two phases, $|\mu| > 2|t|$ (trivial) and $|\mu| < 2|t|$ (non-trivial phase), were illustrated here with special choices for the parameters which made the analysis quite straightforward. However, if we move away from the limiting cases outlined above, we will have interactions in the chain which couple both operators on the same lattice site and on different lattice sites. The localization of the zero mode to the ends of the chain spreads out over the bulk lattice sites, and decays exponentially in the length of the chain. [20]

3. 1D chain on a superconductor

The model we present here concerns scalar impurities on a two-dimensional p-wave superconductor. The treatment is based on the research that went into Ref. [3]. We will later reduce the model to a one-dimensional chain. There is a possibility of higher energy gaps than in full two-dimensional systems, and such topological subsystems may offer better access to the exotic particle excitations. By also taking into account energies far away from the gap center, our aim is to derive a theoretical foundation which will allow us to accurately calculate the spectrum all subgap energies.

In Sec. 3.1, we restrict our model to a periodic lattice, which will allow us to make analytical progress in reciprocal space due to the translational symmetry. Then we present the topology of the system in Sec. 3.2. We first consider a spinless superconductor, and in Sec. 3.3, we generalize our work to the corresponding system including spin, making use of the following treatment.

The system under consideration is described by the Bogoliubov-de Gennes (BdG) Hamiltonian[1]

$$\mathcal{H} = \xi_{\mathbf{k}}\tau_z + \Delta(k_x\tau_x - k_y\tau_y) + U\sum_i \tau_z\delta(\mathbf{r} - \mathbf{r}_i), \tag{3.1}$$

where $\xi_{\mathbf{k}} = k^2/2m - \mu$ is the kinetic energy of the electrons, $\mu = k_F^2/2m$ is the chemical potential, and m denotes the effective mass of the electrons. Δ is, as

[1]While this is a *Hamiltonian density*, we will follow the usual convention of just calling this the Hamiltonian.

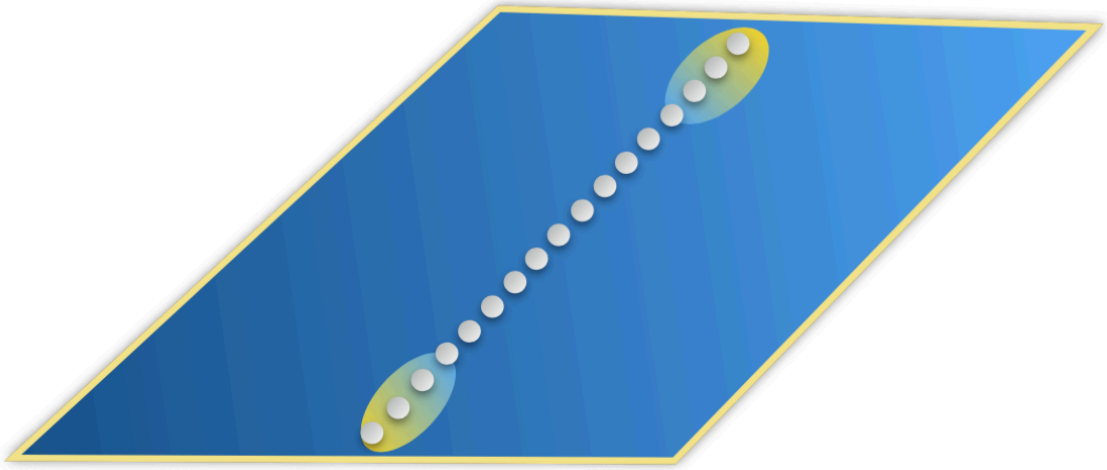

Figure 3.1: One-dimensional chain of scalar potential impurities on top of a p-wave superconductor. This system will be shown to host topological phases, and their nature is reflected in the bound states localized at the ends of the chain.

before, the gap of the underlying superconductor, and U is the potential of the impurities. The Pauli matrices τ_i, $i = x, y, z$, act in the particle-hole space; later we will also introduce the symbols σ_i for the same matrices acting in spin space. The Hamiltonian (3.1) is expressed in the Nambu basis $\Psi(\mathbf{r}) = (\psi(\mathbf{r}), \psi^\dagger(\mathbf{r}))^T$. The energy spectrum can be solved by inserting (3.1) into the BdG equation $\mathcal{H}\Psi = E\Psi$, which we can rearrange to obtain

$$\left[E - \xi_{\mathbf{k}}\tau_z - \Delta(k_x\tau_x - k_y\tau_y)\right]\Psi(\mathbf{r}) = U\sum_j \tau_z\delta(\mathbf{r} - \mathbf{r}_j)\Psi(\mathbf{r}_j), \tag{3.2}$$

where we have isolated all impurity terms to the right hand side. Moving to momentum space using $\Psi(\mathbf{r}) = \int [d\mathbf{k}/(2\pi)^2] e^{i\mathbf{k}\cdot\mathbf{r}}\Psi_{\mathbf{k}}$, we obtain

$$\left[E - \xi_{\mathbf{k}}\tau_z - \Delta(k_x\tau_x - k_y\tau_y)\right]\Psi_{\mathbf{k}} = U\sum_j e^{-i\mathbf{k}\cdot\mathbf{r}_j}\tau_z\Psi(\mathbf{r}_j). \tag{3.3}$$

Now, in order to obtain $\Psi_{\mathbf{k}}$ by itself, we simply multiply by the inverse of the matrix preceding it. Then, defining the following shorthand notation,

$$J_E(\mathbf{r}) = U\int \frac{d\mathbf{k}}{(2\pi)^2}\left[E - \xi_{\mathbf{k}}\tau_z - \Delta(k_x\tau_x - k_y\tau_y)\right]^{-1} e^{i\mathbf{k}\cdot\mathbf{r}} \tag{3.4}$$

we move back to real space, evaluate the obtained equation at $\mathbf{r} = \mathbf{r}_j$, leading to

$$\left[1 - J_E(\mathbf{0})\tau_z\right]\Psi(\mathbf{r}_i) = \sum_{j\neq i} J_E(\mathbf{r}_{ij})\tau_z\Psi(\mathbf{r}_j), \tag{3.5}$$

where $\mathbf{r}_{ij} = \mathbf{r}_i - \mathbf{r}_j$, and where we have for convenience separated the term $j = i$ from the sum. We will not bother with the technicalities any further than this, and we will move the rest of the details to the appendices. Note that we have now formulated the original BdG eigenvalue problem as an eigenvalue problem for N coupled 2×1 spinors Ψ_j. The positions for the N impurities have thus far been completely arbitrary; now we will restrict the problem to a one-dimensional chain of impurities. We do this by simply setting $y = 0$ for all $\mathbf{r}_j$ in the above expressions. The calculations for the integrals J_E are found in Appendix A; here we just present the results: Defining $\gamma = 1 + \frac{\Delta^2}{v_F^2}$, $\beta = \Delta^2 k_F^2 - \gamma E^2$, and $\tilde{\Delta} = \Delta^2 \frac{k_F}{v_F \gamma}$, the obtained expressions can be reduced to

$$J_E(x = 0) \approx \frac{\alpha}{\sqrt{\beta}}\left[\tilde{\Delta}\tau_z - E\right] \tag{3.6}$$

$$\begin{aligned} J_E(x \neq 0) \approx \alpha\Bigg[&\frac{-E}{\sqrt{\beta}}\,\mathrm{Re}\,(\Phi_0) + \left(\frac{\tilde{\Delta}}{\sqrt{\beta}} - \frac{1}{\gamma}\,\mathrm{Im}\,(\Phi_0)\right)\tau_z \\ &- \frac{i\Delta\,\mathrm{sgn}(x)}{\gamma}\left(\frac{1}{v_F}\left[\frac{2}{\pi} - \mathrm{Re}\,(\Phi_1)\right] + \frac{k_F}{\sqrt{\beta}}\,\mathrm{Im}\,(\Phi_1)\right)\tau_x\Bigg] \end{aligned} \tag{3.7}$$

where $\alpha = \pi\nu_0 U$ characterizes the strength of the potential and where we have defined the shorthand $\Phi_n = I_n(x\Omega) - \mathbf{L}_n(x\Omega)$, with $\Omega = \frac{1}{\gamma}\left(\frac{\sqrt{\beta}}{v_F} + ik_F\right)$. Here $I_n(x)$ and $\mathbf{L}_n(x)$ are the modified Bessel and Struve functions of the first kind, respectively, and v_F is the Fermi velocity.

After inserting the obtained expressions (3.6) and (3.7) for the integrals J_E into Eq. (3.5), writing it in a matrix form, and grouping together terms with the same prefactors, we finally arrive at

$$\frac{1}{\sqrt{\beta}}\begin{pmatrix} (\varepsilon - 1)A & B \\ B & (\varepsilon + 1)A \end{pmatrix}\Psi = \begin{pmatrix} C - \alpha^{-1} & D \\ D & \alpha^{-1} - C \end{pmatrix}\Psi, \tag{3.8}$$

where we have defined a reduced energy $\varepsilon = E/\tilde{\Delta}$, $\Psi^T = [\Psi(x_1)^T \dots \Psi(x_N)^T]$ is a $2N \times 1$ spinor, and the expressions for the $N \times N$ Hermitian submatrices A, B, C, D are given in Appendix A. We have a $2N \times 2N$ matrix structure since the N impurity sites are each described by two-component BdG spinors $\Psi_j = \Psi(x_j)$. Eq. (3.8) is a non-linear eigenvalue problem describing a long-range tight-binding model, and the hopping elements between different impurity sites decay asymptotically as $\exp(-r/\xi_E)/\sqrt{k_F r}$ for coherence length $\xi_E = \gamma v_F/\sqrt{\beta}$. We also note that for low energies $\xi_E \approx \gamma v_F/|\Delta| k_F \equiv \gamma\xi$. The full solution to the matrix eigenvalue problem (3.8) consists of $2N$ energy states and their corresponding eigenspinors. The mathematical structure of the problem is closely related to those studied in Refs. [22–24] for magnetic chains. The non-linear energy dependence through β and Φ_n complicates the solution considerably, but as we will see in the later analysis, these obstacles can also be circumvented, and we maintain a high precision for the energy solutions.

3.1 Momentum space analysis

Up to Eq. (3.5), the system was not specific to any particular arrangement of the impurities, and Eq. (3.8) only demands that the impurities are aligned along one direction. While this is more general, it is hardly a helpful feature of the system. As with any quantum mechanical problem involving many particles at arbitrary locations, finding an exact solution specific to all constituents involved is implausible at best. By considering a periodic lattice of impurities, we gain translational invariance in the system, which can be exploited by going over to reciprocal space. The goal is to attempt to solve the eigenvalue problem given by Eq. (3.8). To this end, we define the Fourier transforms of the submatrices, given by

$$a_k = \sum_j A_{ij} e^{ika(i-j)}, \tag{3.9}$$

with analogous expressions for b_k, c_k, and d_k. Looking at the explicit expressions for the submatrices of Eq. (3.8), we see that they have energy-dependent parts only within the special functions Φ_n. This separation of energy dependence into factors outside the submatrices makes the transformation into reciprocal space straightforward. We simply end up with

$$\frac{1}{\sqrt{\beta}}\begin{pmatrix}(\varepsilon-1)a_k & b_k \\ b_k & (\varepsilon+1)a_k\end{pmatrix}\psi_k = \begin{pmatrix}c_k-\alpha^{-1} & d_k \\ d_k & \alpha^{-1}-c_k\end{pmatrix}\psi_k, \tag{3.10}$$

with the real-space submatrices replaced by their Fourier-transformed counterparts as defined above. It is now possible to express the non-linear eigenvalue equation in a more accessible form. Moving all terms in the above equation to the left hand side, we obtain an equation of the form $G_k^{-1}\psi_k = 0$, with

$$G_k^{-1} = \begin{pmatrix}(\varepsilon-1)a_k - \sqrt{\beta}(c_k-\frac{1}{\alpha}) & b_k - \sqrt{\beta}d_k \\ b_k - \sqrt{\beta}d_k & (\varepsilon+1)a_k + \sqrt{\beta}(c_k-\frac{1}{\alpha})\end{pmatrix}. \tag{3.11}$$

The energy bands can now be solved from the condition $\det(G_k^{-1}) = 0$ for each k. The steps are detailed in Appendix B; here we just provide the closed form equation for the energy bands E_k:

$$P_{2,k}\beta(E_k) + P_{1,k}\sqrt{\beta(E_k)} + P_{0,k} = 0. \tag{3.12}$$

with the expressions for the coefficients P_n also moved to the appendix. Clearly, this equation is easily solved for the energies by use of the quadratic formula, and subsequent transformation from $\beta(E)$ to E. However, we should note that by simply presenting this equation as-is, we would gloss over the unpleasant energy dependence hidden in the coefficients P_n. They originate from the integral (3.7), or more precisely, in the real part of Ω which sits inside the special functions $\Phi_n = \Phi_n(x\Omega)$. We deal with this problem by simply setting the energies inside the coefficients P_n to zero as a first approximation. We can obtain the true eigenvalues using an iterative process, where the resultant energies E_i obtained by solving Eq. (3.12) are used as

the new starting points in the coefficients P_n. However, this process converges so quickly, that the change in the energies turns out to be essentially negligible. Such a procedure is employed in Ref. [24], with a detailed discussion for the interested reader. So the effect of neglecting the inner energy dependencies all but evaporates, and we can safely set $E = 0$ in the coefficients of Eq. (3.12), and directly solve for the energy eigenvalues using the good old quadratic formula.

Now that we have solved the eigenvalue problem, we can compute the energy gap of the system in order to estimate the robustness of the topological phases hosted by this model. Note that had we employed a low-energy limit in the above analysis, the obtained energy gap would only be accurate for very low energies, and higher-energy solutions would be somewhat arbitrary and could not be relied on for an accurate estimate of the energy gap. Since β is a function of E^2, we see directly that the energy solutions come in pairs $\pm E_k$, as is expected due to the particle-hole symmetry of the system.

3.2 Topology

Use of the Hamiltonian is central to the investigation of the topological character of the system. However, above we formulated our problem as a non-linear eigenvalue problem, so it is not immediately obvious what our Hamiltonian should be (cf. Eq. (3.8)). Luckily, we can study the topological effects using an effective Hamiltonian. We follow the treatments of Refs. [23, 24]. We would like the effective Hamiltonian to possess the same topological properties as our system, and so, as discussed below, we can define it through Eq. (3.11) as $H_{\text{eff}} \equiv G^{-1}(0)$. Substitution into the definition of G^{-1} immediately gives

$$H_{\text{eff}} = \left[\tilde{a}_k + |\Delta|\, k_F \left(\tilde{c}_k - \frac{1}{\alpha}\right)\right] \tau_z + \left[|\Delta|\, k_F \tilde{d}_k - \tilde{b}_k\right] \tau_x, \tag{3.13}$$

where we have introduced the notation $\tilde{a}_k = \lim_{E\to 0} a_k$ for all $a_k, ..., d_k$. There are a few key properties to appreciate about H_{eff}. First, it clearly has a simpler mathematical structure than G^{-1}, making analytical and numerical computation a significantly easier task. Second, by construction, all of its zero-energy solutions are also (zero-energy) solutions of the original Hamiltonian. This is to say that the gap closings of the effective Hamiltonian and the parent model coincide exactly. Any borders between topologically different regions are thus the same for both models. So even though we have spoiled the energy dependence of H_{eff} as a predictor of the energy eigenvalues of the system, it is still useful in studying its topological features.

Next, we need to identify the relevant symmetries of the model if we are to extract its topological properties, and ultimately, a topological phase diagram. The particle-hole symmerty, which emerged automatically once we employed the BdG formalism in the above analysis, puts our system in the Altland-Zirnbauer class D [25,26]. Thus there exists a $\mathbb{Z}_2$-valued topological invariant for this system. But since we reduced the model to be effectively one-dimensional, we now also have a chiral symmetry in our system. This is manifested through the anti-commutation relation $\{\mathcal{C}, \mathcal{H}\} = 0$ for some operator $\mathcal{C}$ called the chiral symmetry operator. This puts our model in the BDI class, which supports a $\mathbb{Z}$-valued topological invariant. The $\mathbb{Z}_2$-valued invariant distinguishes phases with different fermion parity [20], which we will also see in Sec. 3.4 when we present the results for the two different topological invariants.

We begin the discussion with the $\mathbb{Z}$-valued invariant. For 1D systems, a topological invariant called the *winding number* can be calculated through the formula

$$\nu = \frac{1}{4\pi i} \int_{-\pi/a}^{\pi/a} \mathrm{d}k \ \mathrm{tr}\left[\mathcal{C} H^{-1} \partial_k H\right], \tag{3.14}$$

where $\mathcal{C}$ is the chiral symmetry operator mentioned above. [27] Now, instead of using a more complicated Hamiltonian describing the system, we can use the effective

Hamiltonian H_{eff}. As discussed above, this does not change the result, but due to its simpler form, this is a computationally more efficient method. In this case, our chiral symmetry operator is $\mathcal{C} = \tau_y$. We postpone the presentation of the topological phase diagrams to Sec. 3.4, but let us mention that formula (3.14) gives us three distinct topological invariants: $\nu = 0, -1, -2$. Now, the magnitude of the winding number represents the number of Majorana bound states (MBSs) localized at the ends of the chain; $\nu = 0$ corresponds to the topologically trivial phase. We will justify this interpretation in Subsec. 3.4.1. Since only the magnitude of ν is of any importance, we clearly have a sign ambiguity in Eq. (3.14). Let us make the purely aesthetic change – which will manifest itself only in the figures presented below – and redefine our topological invariant $\nu \to -\nu$:

$$\nu = \frac{i}{4\pi} \int_{-\pi/a}^{\pi/a} \mathrm{d}k \ \mathrm{tr} \left[\mathcal{C} H^{-1} \partial_k H \right]. \tag{3.15}$$

It is important to note that for systems which arrive at both positive and negative topological invariants, opposite invariants are not at all equivalent. The invariants could for instance correspond to edge states moving around a 2D surface in *opposite* directions. We make this change because the parameter regions investigated in our work only attain winding numbers of the same sign. It is unclear whether our model could attain topological invariants of both signs; perhaps only at unphysical regions in the parameter space. Nonetheless, the sign of the topological invariant can always be flipped *globally*.[2]

As mentioned above, our system supports a $\mathbb{Z}_2$-valued topological invariant, which measures fermion parity. It can change its value only when the energy gap closes at points $k = 0, \pi/a$. We can now obtain the boundaries between different phases of the $\mathbb{Z}_2$ invariant by imposing the gap closing condition on the effective Hamiltonian H_{eff}, since, by construction, it is just G^{-1} with all its energy dependen-

[2]such that all winding numbers, i.e. all points in the parameter space, are affected by this change.

cies set to zero. This provides an independent consistency check for the boundaries where the winding number (3.15) changes parity. Now, since the submatrices B, D of Eq. (3.8) (given in Appendix A) are antisymmetric matrices, we know that the Fourier transformed coefficients $\tilde{b}_k, \tilde{d}_k$ vanish identically at the points $k = 0, \pi/a$. Thus we obtain our phase boundary condition in the form[3]

$$\alpha^{-1} = \left(\frac{\tilde{a}_k}{|\Delta|\, k_F} + \tilde{c}_k \right) \Bigg|_{k=0,\pi/a} \tag{3.16}$$

Keeping other parameters constant, we can then plot this as a curve $\alpha = \alpha(k_F a)$ together with the winding number $\nu = \nu(\alpha, k_F a)$, and as we will see, the two different ways of establishing the parity-changing phase boundaries are consistent with one another.

3.3 Spinful superconductor

So far we have considered a system consisting of a *spinless* chiral p-wave superconductor decorated with potential impurities, but in this section we will generalize our results to the model including spin. We consider both a chiral and a helical superconductor. We parametrize the 2D p-wave models by writing the BdG Hamiltonian of the superconductor as

$$\mathcal{H}_{\mathrm{SC}} = \begin{pmatrix} \xi_{\mathbf{k}} & \Delta \mathbf{d} \cdot \boldsymbol{\sigma} \\ \Delta (\mathbf{d} \cdot \boldsymbol{\sigma})^\dagger & -\xi_{\mathbf{k}} \end{pmatrix}, \tag{3.17}$$

where $\mathbf{d}$ determines the spin structure of the superconductor, and $\boldsymbol{\sigma}$ is now a vector of the matrices σ_i, which are Pauli matrices acting in spin space.

The first case we consider is $\mathbf{d} = (0, 0, k_x + ik_y)$, which describes a chiral superconductor. It is the main candidate for describing the pairing in Sr_2RuO_4 [28].

[3] Presumably due to a technical error, this equation was published with a typographical mistake in Ref. [3], but appears here in the correct form.

Substituting the **d**-vector into Eq. (3.17) and including the impurity terms as before, we obtain

$$\mathcal{H}_{\rm c} = \xi_{\mathbf{k}}\tau_z + \Delta\sigma_z(k_x\tau_x - k_y\tau_y) + U\sum_i \tau_z\delta(\mathbf{r}-\mathbf{r}_i). \tag{3.18}$$

Evidently, this Hamiltonian has the matrix structure of that of two spinless Hamiltonians as the two blocks, but they differ in the sign of Δ. Exactly because $\mathcal{H}_{\rm c}$ is diagonal in spin space, we can generalize the results of the previous sections in a straightforward manner. Indeed, the calculations proceed almost identically for the spinful case. In fact, just by looking at Eq. (3.13) and checking the explicit expressions for the submatrices in Eqs. (A.20)-(A.23), we see that the left and the right terms are symmetric and antisymmetric, respectively, with respect to the change $\Delta \to -\Delta$. This immediately gives us the effective chiral Hamiltonian

$$\tilde{H}_{\rm c,eff} = \left[\tilde{a}_k + |\Delta|\, k_F\left(\tilde{c}_k - \frac{1}{\alpha}\right)\right]\tau_z + \left[|\Delta|\, k_F\tilde{d}_k - \tilde{b}_k\right]\tau_x\sigma_z. \tag{3.19}$$

Now we can define our chiral symmetry operator to be $\mathcal{C} = \tau_y\sigma_z$, and so immediately see that the winding number (3.15) acquires the change $\nu \to 2\nu$, since the contributions from each block are simply added together. So the topological invariants are merely doubled, and thus the topological phase diagrams to be presented in Sec. 3.4 remain identical to the spinless case.

Now, it is possible to access additional winding numbers through further interaction terms in the Hamiltonian. We can do this by lifting the spin degeneracy while keeping the chiral symmetry intact, e.g. by a Zeeman field $\mathcal{H}_{\rm c} \to \mathcal{H}_{\rm c} + B\sigma_x$. To see this, we note that using the unitary operator $\mathcal{U} = \exp(i\pi\tau_z\sigma_y/4)$, we can transform just the new term to obtain

$$\mathcal{H}_{\rm c}^B = (\xi_{\mathbf{k}} + B\sigma_z)\tau_z + \Delta\sigma_z(k_x\tau_x - k_y\tau_y) + U\sum_i \tau_z\delta(\mathbf{r}-\mathbf{r}_i). \tag{3.20}$$

This is due to the anticommutativity of the Pauli matrices, which neatly leaves all the other terms invariant in the unitary transformation $\mathcal{H}_{\rm c} \to \mathcal{U}\mathcal{H}_{\rm c}\mathcal{U}^\dagger$. Evidently, the addition in the first term amounts to the change of the chemical potential $\mu =$

$k_F^2/2m \to k_F^2/2m \mp B$, or simply the shift[4] $k_F \to \sqrt{k_F^2 \mp 2mB}$. Now the boundaries between topologically distinct regions for the separate blocks are shifted in different directions in the parameter space. As discussed above, the winding number formula (3.15) effectively adds together the "bare" winding numbers for the different blocks, and so the resulting topological invariant now also attains the odd values $\nu = 1, 3$.

For the other spinful case we consider a helical superconductor, described by the in-plane vector $\mathbf{d} = (k_x, k_y, 0)$. Substitution again yields a new Hamiltonian of the form

$$\mathcal{H}_{\mathrm{h}} = \xi_{\mathbf{k}}\tau_z + \Delta\tau_x(k_x\sigma_x + k_y\sigma_y) + U\sum_i \tau_z\delta(\mathbf{r} - \mathbf{r}_i). \tag{3.21}$$

We can now perform a change of basis $(\psi_\uparrow, \psi_\downarrow, \psi_\downarrow^\dagger, -\psi_\uparrow^\dagger)^T \to (\psi_\uparrow, \psi_\uparrow^\dagger, \psi_\downarrow, \psi_\downarrow^\dagger)^T$ to obtain our helical Hamiltonian in the form

$$\mathcal{H}_{\mathrm{h}} = \xi_{\mathbf{k}}\tau_z - \Delta\sigma_z(k_x\tau_x + k_y\sigma_z\tau_y) + U\sum_i \tau_z\delta(\mathbf{r} - \mathbf{r}_i) \tag{3.22}$$

which differs from the previous chiral Hamiltonian (3.18) only in the sign of Δ, and in the σ_z multiplying k_y. Following the derivation of the non-linear eigenvalue problem (3.8) given in Appendix A, we see that the contribution from the k_y term vanishes when we restrict our system of impurities to be one-dimensional. Thus the effective difference of $\mathcal{H}_{\mathrm{h}}$ to the bare chiral Hamiltonian $\mathcal{H}_{\mathrm{c}}$ is just the change $\Delta \to -\Delta$. This difference is mostly inconsequential, so for practical purposes, we are now dealing with the same Hamiltonian. Therefore the above discussion on the energy gaps and the topological phase diagrams extends to $\mathcal{H}_{\mathrm{h}}$ as well; they coincide with the spinless case. Again, the winding number is simply doubled, $\nu \to 2\nu$, resulting in the same three distinct topological phases as above.

We can again access the odd topological invariants $\nu = 1, 3$ by applying a magnetic field in the z-direction. When we apply the same change of basis as above

[4]We stick to the convention of the $\pm$-sign that the upper sign is, in some obvious sense, "first" in order. In this case, the upper signs correspond to the upper left blocks of the matrix.

on an additional term $B\sigma_z$, we obtain the helical Hamiltonian in the form

$$\mathcal{H}_{\mathrm{h}}^{B} = (\xi_{\mathbf{k}} + B\sigma_z)\tau_z - \Delta\sigma_z(k_x\tau_x + k_y\sigma_z\tau_y) + U\sum_i \tau_z\delta(\mathbf{r} - \mathbf{r}_i), \tag{3.23}$$

that is, the desired term is obtained automatically. Thus it has the same effect on the phase diagrams as we saw above for the chiral case, shifting the Fermi wave number $k_F \to \sqrt{k_F^2 \mp 2mB}$.

There is still one more thing to note about the magnetic fields applied to the two spinful Hamiltonians. In the chiral case, we could have chosen any magnetic field that points in the xy-plane. This is because we can rotate it back to the x-direction by use of a unitary transformation, and then obtain the same effect as we saw above. To see this, just note that $e^{i\frac{\varphi}{2}\sigma_z}B(\sigma_x\cos\varphi + \sigma_y\sin\varphi)e^{-i\frac{\varphi}{2}\sigma_z} = e^{i\varphi\sigma_z}B(\sigma_x\cos\varphi + \sigma_y\sin\varphi) = B\sigma_x$. For the helical case, however, this is not the case anymore. The magnetic field must point in the z-direction; otherwise we will either not achieve the splitting of $k_F \to k_F^{\pm}$, or we will destroy some of the symmetries necessary for achieving non-trivial topology in our model.

3.4 Results

In this section, we present the topology of the one-dimensional chain of potential impurities, presenting first the energy gap diagram, and then the corresponding topological phase diagram. We also give the phase diagram for the case of a spinful superconductor, and are able to access additional topological phases, as was detailed in Sec. 3.3. In Subsec. 3.4.1, we justify the physical interpretation of the winding number invariant as the number of Majorana bound states localized at the ends of the chain.

We commented on the different symmetry classes of this model in Sec. 3.2, and we expect the system to support two distinct topological invariants that are closely interrelated. The main focus is the $\mathbb{Z}$-valued topological invariant given in Eq. (3.15),

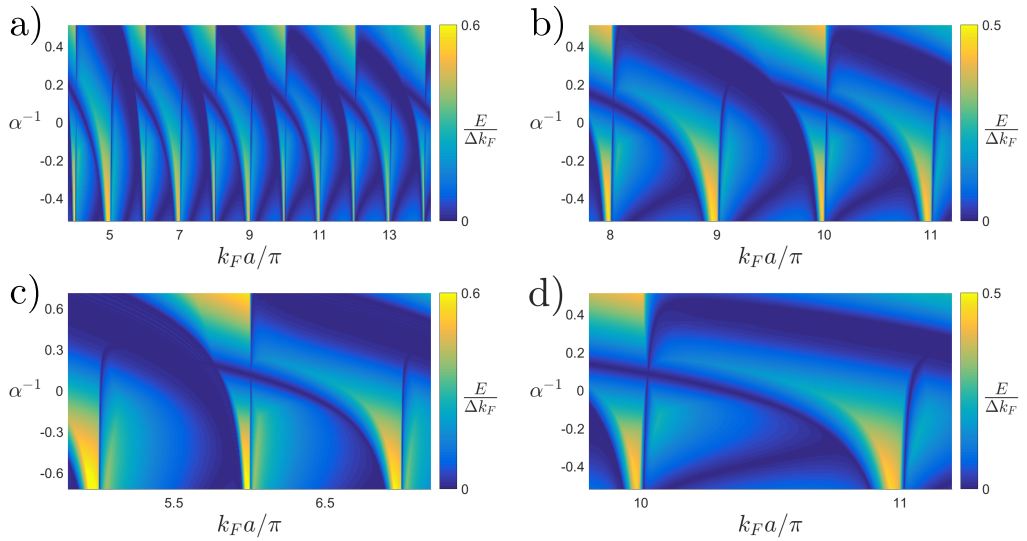

Figure 3.2: a) Lowest positive energy eigenvalue as a function of $k_F a$ and α^{-1}. The values used for the coherence length is $\xi = 20a$, with $\Delta/v_F = 1/(k_F\xi)$. For this plot, we have set $v_F = 100$. b) Same as in a) except for a narrower range of $k_F a$ values. The plots in c) and d) are the same as in a) and b), but for yet other parameter ranges, and with $v_F = 15$.

since it gives the topological character of each phase, while the information extracted from the other invariant only reveals the boundaries between phases of different parity. However, as mentioned before, it serves as an important consistency check for the topological phase diagram presented below.

The energy eigenvalues of the system were calculated in Sec. 3.1, with the final result for the energy bands given in Eq. (3.12). The gap provides important information regarding the robustness of the topological phases. In Fig. 3.2, we have plotted the minimum energy solution $\min_k |E_k|$ as a function of $k_F a$, where a is the lattice constant of the impurity chain, and of the dimensionless impurity strength $\alpha = \pi\nu_0 U$. From the figure we can see that the system has distinct gapped regions which are separated by gap closings. Note that the energy gap can reach a significant fraction of the underlying superconducting gap, even more than $\sim 0.5\Delta k_F$ in regions which, as we will see shortly, turn out to be topological. In particular, these values are so high as to be well outside the validity of any low-energy approximations.

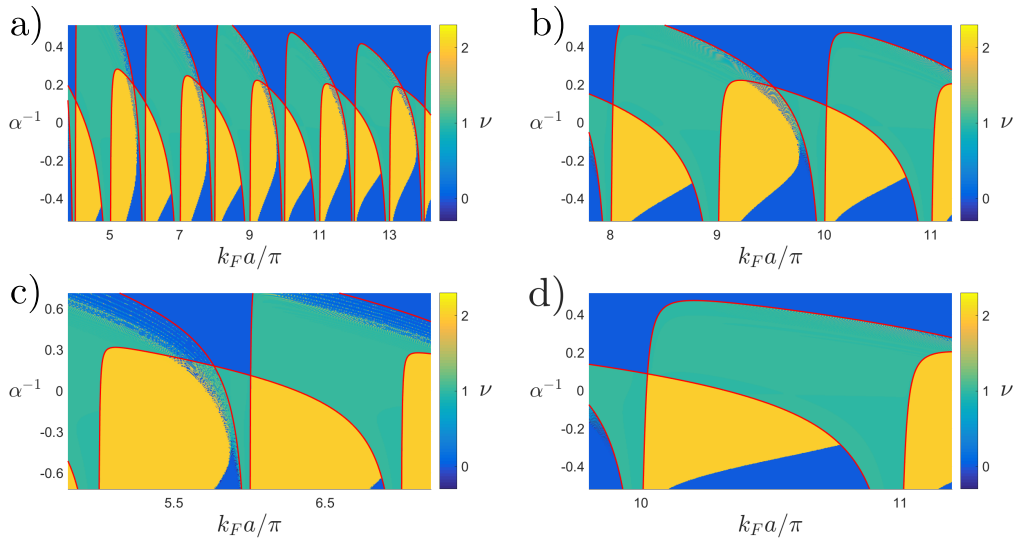

Figure 3.3: a)-d) Winding number invariant as a function of $k_F a$ and α^{-1}, over equivalent parameter ranges as in Fig. 3.2; the fixed parameters of these subfigures correspond exactly to the parameters used for the energy gap calculations. The analytical k-space solution (see Eq. (3.16)) for boundaries between different parity phases is given by the red graphs.

Upon inspection, we notice a peculiarity in the plots of Fig. 3.2. Instead of α itself, the plots are constructed in terms of α^{-1}, so we ought to discuss the limit $\alpha^{-1} \to 0^{\pm}$, corresponding to an infinite attraction and repulsion, respectively. The spectrum is continuous across this limit, which is highly counterintuitive. This feature stems from the properties of the single-impurity bound states, which coincide in the limit of infinite repulsion and attraction.

In Fig. 3.3, we have plotted the winding number (3.15) as a function of the same parameters as the energy gap diagram Fig. 3.2, with the chiral symmetry operator $\mathcal{C} = \tau_y$ for the spinless case. As mentioned above, we expect the topological invariant to be $\mathbb{Z}$-valued, and we find for it three distinct values: $\nu = 0, 1, 2$. These winding numbers each correspond to the number of MBSs located at the ends of finite chains, as we will see below. In the same figure, we have also included the $\mathbb{Z}_2$-valued invariant. It is seen as a red curve on the boundaries between the different

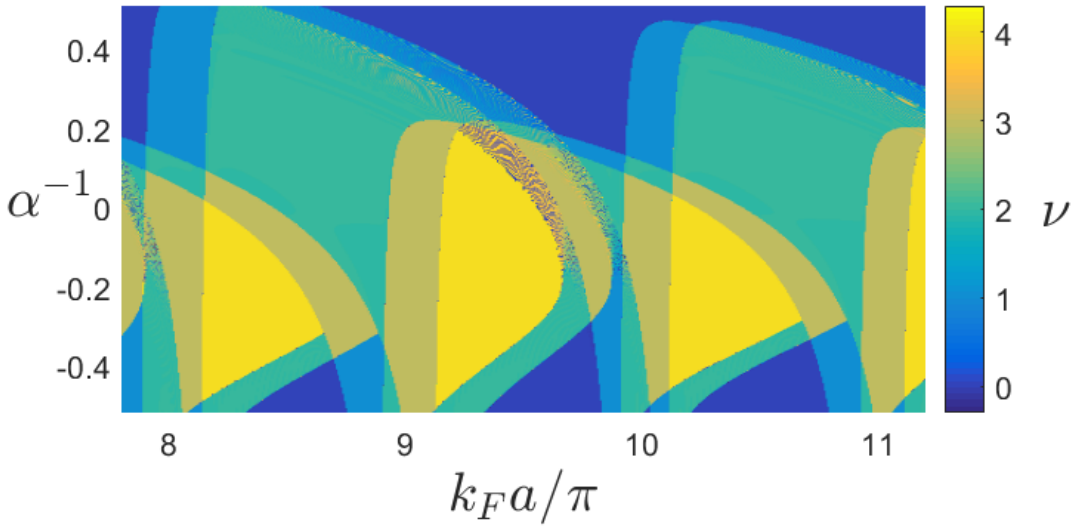

Figure 3.4: Topological phase diagram for the case of a spinful superconductor and an applied Zeeman field of magnitude B; as detailed in Sec. 3.3, this figure represents both chiral and helical superconductors. The range of parameter values corresponds to Fig. 3.3b), and the parameters are also identical, except additionally, $2Bm = 8 \cdot 10^3/\xi^2$.

phases, but only between those that have different parity.[5]

We note that any transition between the different topological phases occurs in the corresponding region of Fig. 3.2 where the energy gap closes, as it should. Now, there is an apparent discrepancy between some topological phases, but this only occurs for regions where the energy gap is extremely low. Here the numerical winding number becomes unreliable. Indeed, in those regions, the topological phase is quite meaningless, since there is practically no separation between the different phases due to the vanishing gap.

It is also evident that whenever $k_F a$ is an integer multiple of π, we have a topological phase boundary between the phases $\nu = 1, 2$ for large negative values of α^{-1}. These may persist infinitely far down, but the breadth of the $\nu = 1$ phase becomes increasingly narrow. As expected, in the low potential limit $U \to 0$ ($|\alpha^{-1}| \to \infty$), the topologically trivial phase starts to dominate.

[5] As seen below, this corresponds to the parity of the winding number ν.

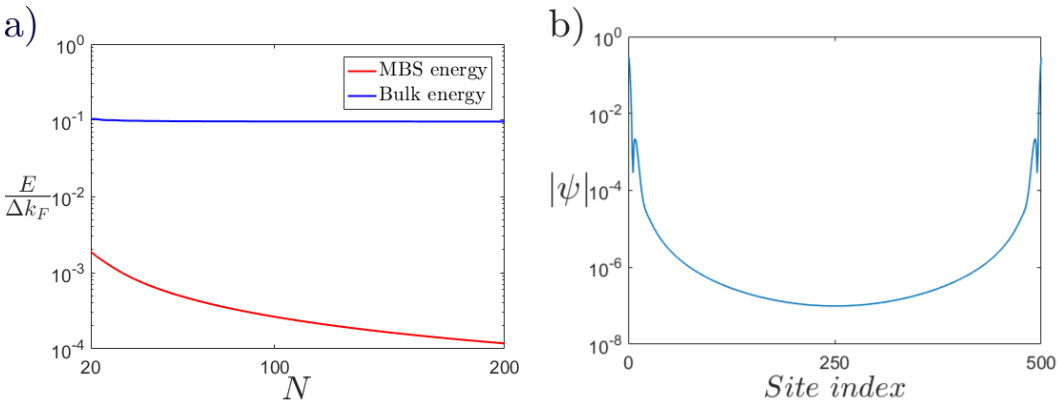

Figure 3.5: a) Dependence of the bulk and MBS energy in the $\nu = 1$ phase on the length N of the impurity chain in blue and red, respectively. b) Localization of the MBS wavefunction in the $\nu = 1$ phase, with chain length $N = 500$. Parameters used in the calculations for these plots are $\Delta/v_F = 1/(k_F\xi)$, with $\xi = 20a$, $k_F a = 8.5\pi$, and $\alpha^{-1} = 0.2$.

In Fig. 3.4, we have plotted the winding number invariant as above, except for a spinful superconductor and an applied Zeeman field, now with $\mathcal{C} = \tau_y\sigma_z$ as the chiral symmetry operator. We showed in Sec. 3.3 that such a field with strength B leads to a shift in the Fermi wave vector $k_F \to \sqrt{k_F^2 \mp 2mB}$, depending on the spin direction. Thus we have two "bare" phase diagrams as in Fig. 3.3b) added together, but shifted in opposite directions. This creates overlaps of different topological invariants, and so we also have clear regions for the winding numbers $\nu = 1, 3$. In particular, the phase boundaries for large negative α^{-1} that seem to approach integer values of $k_F a/\pi$ in Fig. 3.3 are now split evenly on both sides of the corresponding integers. There are some regions where there is significant noise in the winding number between two different phases, but these correspond, as before, to regions of very low energy gap.

3.4.1 Majorana bound states

In Fig. 3.5a), we have plotted the two lowest wave function energies as a function of the length of the chain. Since the next higher energies are almost exactly the

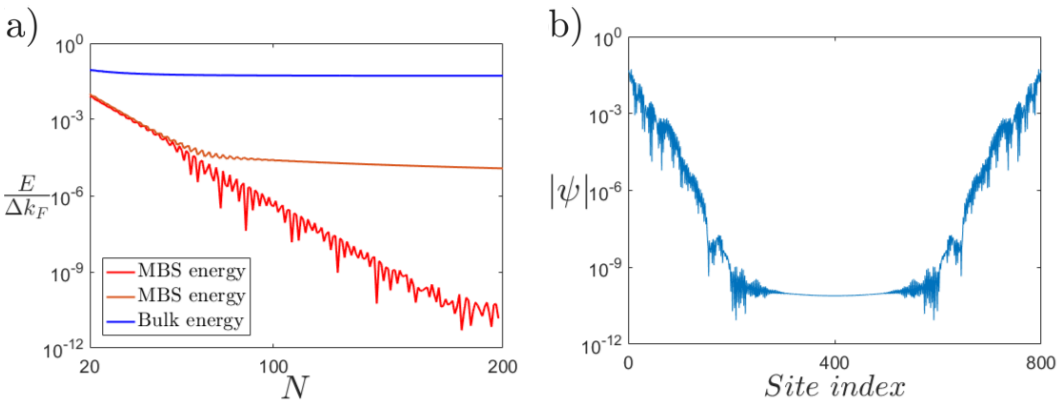

Figure 3.6: a) Same as Fig. 3.5a), except for the $\nu = 2$ phase. The bulk energy dependence is still in blue, and the two MBS energies are in red and orange. b) Localization of the MBS wavefunction in the $\nu = 2$ phase, with chain length $N = 800$. This wave function corresponds to the red, lowest-energy graph seen in a). Parameters used in the calculations for these plots are identical to Fig. 3.5, except that $\alpha^{-1} = -0.2$.

same as for the blue graph, we have simply called it the bulk energy. For infinite systems, we would expect to find one zero-energy mode in this $\nu = 1$ phase, but in finite systems, this is not exactly true. The lowest energy differs from the bulk by at least a few orders of magnitude, and is clearly seen to decrease with increasing chain length, while the bulk energy stays constant. In Fig. 3.5b), we have plotted the magnitude of the wave function at different locations in the chain. The wave function is several orders of magnitude more pronounced at the ends of the chain than throughout the rest of the chain, i.e. it is highly localized to the edges. This is precisely how we expect MBSs to behave, justifying the interpretation of the winding number invariant mentioned above.

In Fig. 3.6, we have plotted similar graphs to Fig. 3.5, except for parameters that correspond to the topological phase with $\nu = 2$. In this case, we have two low-energy modes, one of which has an even smaller energy than in the $\nu = 1$ phase. Up to a chain length of $N \sim 60$, both MBSs have almost exactly the same energy, after which one keeps decreasing faster than the other. The wave function localization plotted in Fig. 3.6b) corresponds to this lower-energy mode, and as before, it is

strongly localized at the ends of the chain. Since the same plot for the other MBS is almost exactly like the plot for the MBS in the $\nu = 1$ phase in Fig. 3.5b), we have omitted it entirely. The general features for the MBSs in the last two figures are the same; the only real difference being that these two characteristics are even more pronounced for the lowest-energy mode in the $\nu = 2$ phase than in the $\nu = 1$ phase.

4. Random lattice topology

The mathematics of random numbers concerns the (un)predictability of events, and is useful in the research of materials that represent real-world counterparts to ideal systems. For instance, a perfect chain of lattice points is perhaps easier to investigate theoretically than it is to even create such a material in the first place. We are always restricted by our ability to manipulate small-scale components, whereas the starting point for a theory-based discussion is that the accuracy of creating such a material is perfect. But what if we could circumvent the whole notion of striving for perfectly engineered systems? The recent work by Agarwala and Shenoy [2] shows that topological phases can be realized in amorphous systems, where the positions of the lattice sites themselves are highly non-regular. This could open up a new approach to realizing topological materials, as the restrictions on the construction of such materials would be a lot looser.

When it comes to engineering materials that have random lattice structures, impurities could ideally be placed on a surface quite casually, without any careful placement[1] – and we should expect our results to be described by a treatment in terms of random numbers. Even if you move around the different lattice points, it is difficult to bring a truly random lattice into a *less* random state. Thus, if we find features that are general to random lattices, the connection between theory and experimental realization would arguably be even stronger than for lattices that

[1] loosely speaking, imagine the spreading of the pellets shot from a shotgun

require high precision.

Previous studies trying to address the problem of disorder in a lattice start out with a crystalline structure, and then impose some small degree of disorder with respect to the fixed lattice sites as a "perturbation". If the obtained lattice differs from a regular one too much, the results will not be valid, since the deviation from the assumed crystalline structure is by no means small. Kobayashi et al. [29] investigated a three-dimensional topological insulator, and found that the topological state shifts to a metal with increasing onsite disorder.

Random numbers can be used to describe amorphous materials, whose lattice configurations are almost completely irregular. Our starting point is the construction of the random lattices included in Ref. [2]. We develop the description of the random lattice as follows. A region of two-dimensional space of area A is filled with uniformly distributed lattice points. The number of sites is N, such that the lattice is characterized by a lattice surface density $\rho = N/A$. Without risk of confusion, we will simply call ρ the density. Now, consider a two-dimensional lattice of size $L_x \times L_y$, where the lattice sites are placed *randomly*.[2] We draw both coordinates x and y for all lattice points from a uniform distribution, i.e. the x-coordinates are described by a stochastic variable $X \sim U(0, L_x)$, and likewise for y. This approach is in stark contrast to disorder calculations, where the lattices sites are fixed in a regular structure, and only deviations are drawn from a random distribution. We note that our work describes a model system of an amorphous material; in particular, no minimum distance between the randomly placed lattice sites is enforced.

In Sec. 4.1, we present the model of topological superconductivity on which our work is based, and in Sec. 4.2, we get into topology of the amorphous system. In Subsec. 4.2.1, we present the topological invariant applied to our system, and

[2] L_x and L_y are integers that stand for the number of lattice sites in a corresponding regular lattice. In fact, the lattice size is given in units of some lattice constant a, which we promptly set equal to 1.

in Subsec. 4.2.2, we discuss the importance of the energy gap for the robustness of the topological phases, and why a direct energy gap approach is not applicable for random lattice configurations. In Sec. 4.3, we present the topological phase diagram of the system, and an example of an edge mode localized at the boundary of the 2D random lattice. Finally, in Sec. 4.4, we briefly discuss the possible mechanism behind the emergence of topological phases in random lattices.

4.1 Model of topological superconductivity

Before we get to the topology of the glassy material mentioned above, we must take a moment to present the model on which our work is based. Our starting point is the main Hamiltonian of Ref. [30] which concerns two-dimensional superconducting surfaces decorated by ferromagnetic adatom lattices. The work culminates in the topological phase diagram – the *Chern mosaic* – and demonstrates that the model supports a rich texture of topologically distinct phases with very high topological invariants.

We include the relevant expressions for the effective low-energy Hamiltonian here, with the background and details moved to Appendix C:

$$H_{mn} = \begin{pmatrix} h_{mn} & \Delta_{mn} \\ (\Delta_{mn})^\dagger & -h^*_{mn} \end{pmatrix}, \tag{4.1}$$

where h_{mn} and Δ_{mn} are $N \times N$ blocks, and are given by

$$h_{mn} = \begin{cases} \varepsilon_0, & m = n \\ \dfrac{\Delta}{2}[I_1^-(r_{mn}) + I_1^+(r_{mn})]\langle\uparrow_m \mid \uparrow_n\rangle & \\ \quad + i\dfrac{\Delta}{2}[I_3^-(r_{mn}) - I_3^+(r_{mn})]\left[\langle\uparrow_m |\sigma_x| \uparrow_n\rangle\dfrac{y_{mn}}{r_{mn}} - \langle\uparrow_m |\sigma_y| \uparrow_n\rangle\dfrac{x_{mn}}{r_{mn}}\right], & m \neq n \end{cases} \tag{4.2}$$

and

$$\Delta_{mn} = \begin{cases} 0, & m = n \\ -\dfrac{\Delta}{2}[I_2^-(r_{mn}) + I_2^+(r_{mn})]\langle\uparrow_m \mid \downarrow_n\rangle & \\ \quad - i\dfrac{\Delta}{2}[I_4^-(r_{mn}) - I_4^+(r_{mn})]\left[\langle\uparrow_m |\sigma_x| \downarrow_n\rangle\dfrac{y_{mn}}{r_{mn}} - \langle\uparrow_m |\sigma_y| \downarrow_n\rangle\dfrac{x_{mn}}{r_{mn}}\right], & m \neq n \end{cases} \tag{4.3}$$

Above, $\mathbf{r}_m = (x_m, y_m)$, $r_{mn} = |\mathbf{r}_m - \mathbf{r}_n|$ is the distance between two (Shiba) lattice sites, and likewise x_{mn} and y_{mn} are the corresponding coordinate differences. The definitions of the functions $I_n^{\pm}$ are given in Appendix C. $|\uparrow_n\rangle$, $|\downarrow_n\rangle$ denote eigenstates of the magnetic moments, $\mathbf{S}_m \cdot \boldsymbol{\sigma}|\uparrow_n\rangle = +|\mathbf{S}_m||\uparrow_n\rangle$, and likewise for $|\downarrow_n\rangle$ with the opposite sign, and ε_0 is the onsite energy.

This model supports a vast sea of distinct topologically non-trivial phases. The lattices investigated for the above model in Ref. [30] are regular, and what we embark on next is the analysis of such systems which instead have *irregular* lattice configurations.

4.2 Topology

Since topological phases have previously only been found in cases where you start out with a regular structure, it is certainly a surprise to discover them also in truly random lattices. Before we get to the topology of our random lattice system, we need an appropriate topological invariant to assess the topology. After that we can start investigating the quality of the topological phases, and to see if it is conceivable to realize them in practice. Although it is difficult to answer this question directly, we find strong arguments for the emergence of topological phases which are protected by a high gap energy.

4.2.1 Bott index

In order for us to analyze the topology of our model, we need to identify a topological invariant, much like the winding number encountered in Sec. 3.2 for our one-dimensional chain of potential impurities. But for the 1D chain, we were able to employ symmetry considerations that allowed simple calculation of the topological invariant – we presented the whole section on topology in k-space. Now, for

our two-dimensional lattices, we have no symmetries whatsoever. The problem with calculating the Chern number that was used in [30] is that for random lattice configurations, numerical calculations can become quite hefty, especially for large system sizes.

Loring and Hastings [31] applied the theory of almost commuting matrices to quantify different topological phases. The treatment is not based on reciprocal space, but on the states occupied in the system, which makes it well suitable for lattices lacking any symmetries.[3] The topological invariant used is called the *Bott index*. It has been thought that it coincides with the Chern number on a torus, if we do not impose any other symmetries on the system. Indeed, D. Toniolo recently submitted a preprint [32] of a proof of the equivalence between the Bott index and the Chern number[4] for such a two-dimensional system.

4.2.2 Energy gap

We will now discuss the robustness of the topological phases found for the random lattices by considering the energies for the nearest unoccupied states in a particular phase. As mentioned in Ch. 3 for the 1D chain, the key feature of the energy gap is that it serves as a measure for how protected a topological phase is. Since we have now been dealing with random lattice structures, for any large enough system there will likely be regions of high density that act as their own "subsystem". The same can happen with regions of low density, which act as a hole, or boundary, for the surrounding lattice. Such a finite part of the system can then have a low-energy

[3] We will not go into further details on the mathematics of almost commuting matrices, since it is beyond the scope of this thesis – instead we just refer the interested reader to the article by Loring and Hastings.

[4] in the thermodynamic limit

edge mode going around it.[5] This affects the calculation of our energy gap, and must be taken into account. We do this by simply including such relevant states in the calculation of the Bott index, up to a certain energy within the gap, and check if the topology of our system has changed. If it has not, then it had no effect on the topology of our lattice, but only on the energy gap.

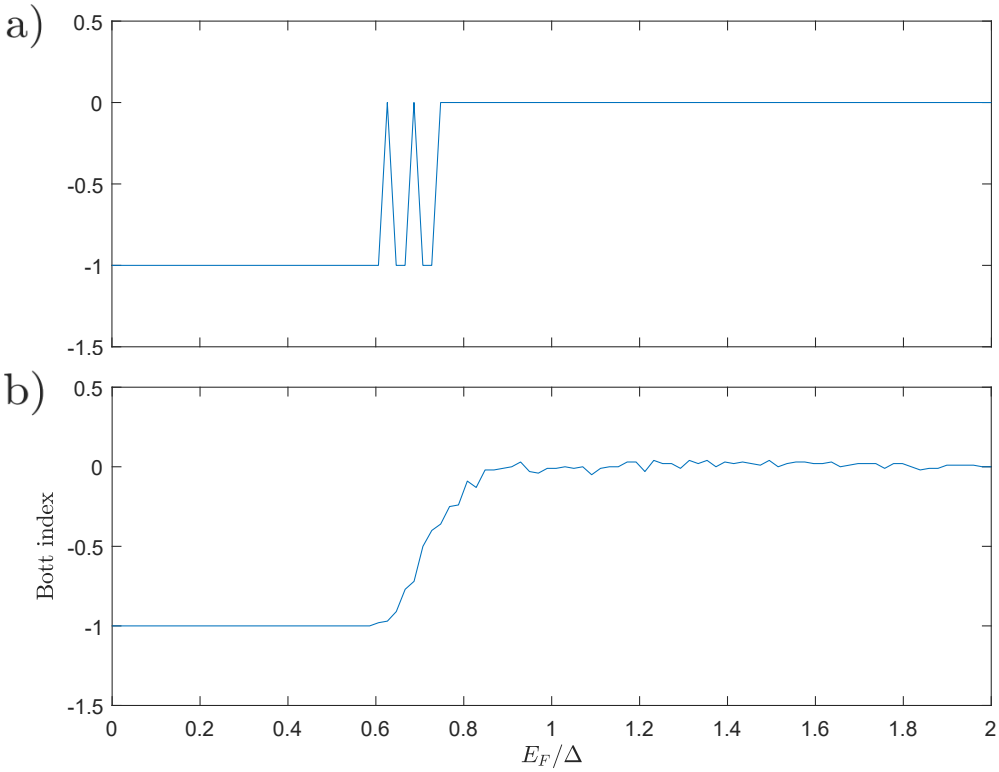

Figure 4.1: a) Bott index as a function of the Fermi energy E_F for a typical configuration of a ferromagnetic random lattice, revealing the mobility gap which is higher than the energy gap. The calculation was performed for a system of size 36×36, with the number of adatom sites $N = 1296$. Parameters used are $\xi = 6$, $k_F a = 4\pi/10$, and $\varepsilon_0 = 0$. b) Same as in a), except averaged over 100 random lattice configurations.

In Fig. 4.1 we have plotted the Bott index as a function of the reduced Fermi energy E_F/Δ. The Bott index for zero Fermi energy is -1, and stays the same for increasing energy up to a value of $\sim 0.7\Delta$. This translates to this particular

[5] In the limit of an infinite (sub)system, the energy of such an edge mode is zero, but for very small subsystems, they can have essentially any subgap energy value.

phase having a mobility gap[6] of ~ 0.7. After increasing the Fermi energy enough, the Bott index becomes zero, i.e. the topology becomes trivial, with some noise at the transition point. The topological phases are the most stable close to the gap center, and we expect the Bott index to go to zero far from the gap center. When the Fermi energy is increased, previously unoccupied states can also be occupied, possibly affecting the topological character of the phase, and ultimately destroying it.

What makes the above graph important is that the energy gap of the system is usually much lower than the mobility gap obtained above. It is, however, important to note that the gaps protecting the topological phases are usually higher than given by the energy solutions. The topological phases are thus more robust than expected based on only an energy gap diagram.

We should note that the graph in Fig. 4.1a) is "unusually clean"; as can be seen in the graph below it, for a generic random lattice configuration, the noise persists long after the phase becomes trivial. In fact, as we increase the Fermi energy further, the quantity calculated above becomes quite meaningless. This is because the random positions of a large number of lattices sites give rise to a huge number of states that are then occupied, and lead to quite arbitrary topological invariants. They by no means describe robust topological phases, but rather "fluctuations" caused by small subsystems, and so high oscillations are expected. What is meaningful is that the Bott index stays exactly constant to a significant fraction of the underlying gap, supporting the conclusion that, for these parameters, the topological phase is robust in a general random lattice.

[6]Henceforth we will forego the Δ in expressions involving energy gaps, and we will just give the energies in units of the underlying superconducting gap Δ.

4.3 Results

In this section, we present the results of the calculations for the model of topological superconductivity on a random lattice. The main result will be the topological phase diagram, which shows that for high enough particle density, the model supports a topologically non-trivial phase. We observe this phase even if we let the local spin directions deviate from the ferromagnetic case.[7] We performed calculations for corresponding phase diagrams, where the configurations for the spin deviations θ_j from the plane are given by Boltzmann weights $e^{-\beta E_Z \cos\theta_j}$. This corresponds to having a Zeeman field E_Z polarizing the spins in a perpendicular direction to the lattice plane, and the spin directions being disordered by thermal fluctuations at inverse temperature β. At $\beta = 10E_Z^{-1}$, the phase diagram stays qualitatively the same as the ferromagnetic case (Fig. 4.2), and there is minimal change to the critical density, which diminishes further with increasing system size.

We will give the density in units of some arbitrary reference point ρ_0, as an increase in the density only means that we reduce the distances between the lattice sites. By a particular choice of this reference density, we can give it a more refined meaning, on which we elaborate below.

In Fig. 4.2, we have plotted the Bott index for a random lattice with ferromagnetic spins, as a function of the lattice site density ρ and the onsite energy ε_0. For low densities, the Bott index oscillates between different integers around zero, but is not non-zero in any larger region of the parameter space. For a different random configuration, the spots of non-zero Bott index may be in very different locations in this parameter subspace, and so the conclusion is clear: The topology of this model is trivial for low densities. When the density becomes larger than the reference

[7] It is not obvious that interactions between the randomly placed magnetic moments are ferromagnetic. For our model system, however, in a large part of the topological region, a ferromagnetic ordering is favored (see the discussion in Ref. [4]).

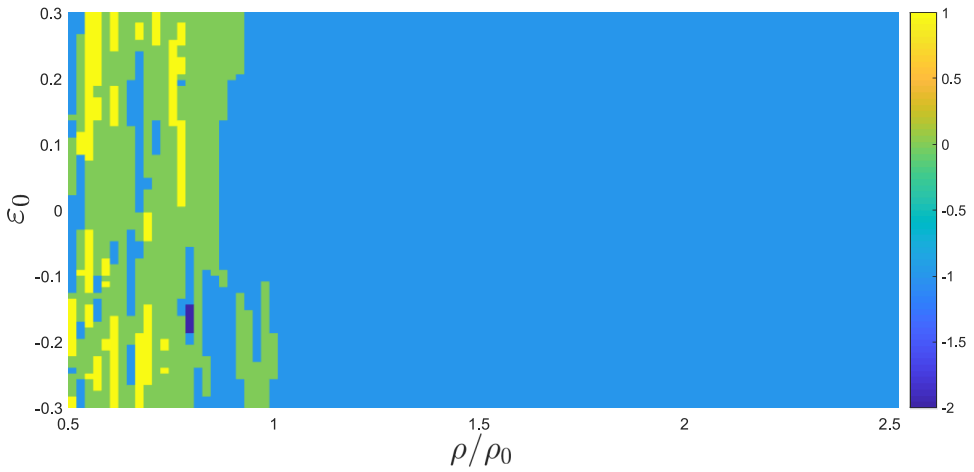

Figure 4.2: Topological phase diagram as a function of the density of lattices sites and the onsite energy ε_0, The calculation was performed for $N = 1296$ randomly placed adatoms with ferromagnetic spins for a system of size 36×36. Parameters used are $k_F a = \pi/2$, $\xi = 6$ and $\lambda = 0.2$.

point ρ_0, the Bott index becomes -1, and stays that way for even larger densities. Thus the random lattice model clearly has some *critical density*, above which the system is in a topologically non-trivial phase.[8] For the parameter regions inspected in this work, no other topological invariants were found, except some fluctuations in the low-density regime. Note that the critical density is almost independent of the onsite energy, with minor deviations for non-zero ε_0. For different random configurations, the deviations may be positioned differently on the ε_0-axis, but for these parameters, the general trend is that this particular ρ_0 defines the critical density. Thus any density higher than that generally leads to the topological phase.

For our purposes, the corresponding energy gap diagram is meaningless, since it only shows the real minimum energy which, as we have seen, is not representative of the mobility gap protecting the topological phase. Indeed, the energy gap diagram includes energies on the order of a few hundredths of the underlying superconducting gap, even far away from any transition point. In principle, one could create a

[8]The ρ-axis is just relabeled to make the appearance of this critical density clearer.

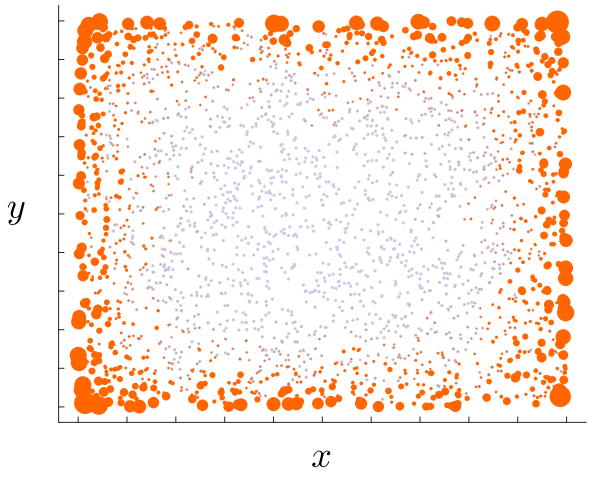

Figure 4.3: Local density of states for a 50×50 square lattice of 2500 randomly distributed ferromagnetic adatom sites, integrated over subgap energies $|E| < 0.1\Delta$. The magnitude of the LDOS is represented through the area of the orange disks, except where the LDOS is negligible, where the lattice sites are represented with a grey dot. Parameters used are $k_F a = \pi/5$, $\xi = 8$ and $\lambda = 0.2$.

mobility gap diagram corresponding to the above phase diagram. However, since the procedure for finding the mobility gap is done for a single point at a time, and essentially requires checking every point by hand, this would require significant amounts of time and large numerical resources. For this treatment, it is enough to conclude that for a point well in the topological phase, the mobility gap protecting the phase can be a large fraction of the underlying superconducting gap. In Subsec. 4.2.2, we determined the mobility gap for a fixed point in the topological phase (see Fig. 4.1). This point corresponds to the point $(\rho/\rho_0, \varepsilon_0) \approx (1.5, 0)$ in Fig. 4.2, and we found for it a mobility gap of about 0.7, roughly two orders of magnitude higher than the corresponding energy gap.

Finally, like the one-dimensional impurity chain discussed in the previous section, also this model exhibits edge modes whenever the topological invariant attains non-zero values. In Fig. 4.3, we have plotted the subgap local density of states (LDOS) in a square lattice with ferromagnetic random lattice sites, in the non-

trivial phase. The magnitude of the LDOS is substantially higher on the boundaries of the square lattice, and is in fact negligible in the middle of the lattice, where each lattice site is represented with a grey dot. This figure shows the emergence of an edge state enclosing this finite system, as is expected in the topological phase. Signatures of these edge modes can be observed in standard scanning tunneling microscopy experiments.

4.4 Discussion

We have already seen that robust topological phases can be hosted by completely random lattices, which is in stark contrast to the usual starting point of regular structures for finding non-trivial topology. As we saw in the previous section, this topological phase persists for high densities independently of the onsite energy ε_0. In fact, for the parameter regions investigated in this work, the non-trivial phase emerges above some *critical density*. It is quite remarkable that we can find such a general feature for realizing topological phases. The procedure for creating random lattices is thus far easier than many regular lattice models proposed to date. This could open up new ways of engineering materials used for quantum computing, and in general allow easier probing of topological phases.

How could we explain what is going on in the random lattice? It seems that we could change the positions of the lattice sites quite freely, and still retain the topological phase. One hypothesis for the observed effect is that the underlying mechanism is reminiscent of *percolation theory*. In this branch of mathematics, the main focus of study are random graphs, and in particular connected clusters within them. When studying percolation theory, one is almost invariably dealing with critical phenomena. The models are mainly controlled by some natural parameter which has a critical value, above (below) which the behavior of the system changes drastically.

Percolation theory can help quantify the spreading of a strain of flu, depending on how infectious the flu is, or the spreading of a forest fire, depending on how far apart the trees are positioned. There is some basic interaction between the individual constituents, and none of them are solely responsible for the state achieved beyond the critical point. In the example of a forest fire, there is some probability that a tree will be "infected" – lit on fire – by a neighboring blighted tree. The problem is then to determine what distances between the trees will lead to fire being lit on a significant portion of the trees, or all of them. [33]

In our case, the variable displaying a critical value is the density. Due to the construction of the model, the particular value of the density is not of importance, but instead, the mere fact that there exists a critical value is meaningful, and it supports percolation theory as a viable possibility. It could be that when it comes to the topological phases of random lattices, there is some fundamental percolation mechanism at play. The topological phases occur when we have edge modes that move on the boundary of the lattice. It is certainly a challenge to describe the problem entirely in terms of percolation theory, since there is no clear way to connect the interaction of a few lattice sites to a certain state of the system.

Future work may be able to bring a new perspective on the problem of non-trivial topology in random lattices. Perhaps this will further enhance our abilities to physically realize topological phases. Further investigation is still needed in order to justify this approach in terms of percolation theory, so at this level, we are not left with much more than speculation.

5. Conclusions

This thesis has been concerned with topological superconductivity in two highly contrasting situations: lattice structures of perfect chains of scalar impurities, and two-dimensional lattices of complete *random* character. Actual engineering of the former is a challenge, as one needs a mechanism for planting potential impurities on top of a superconducting surface with *ideal* precision, and indeed any physical realization will highly depend on the machinery used for its implementation. The latter case concerns a system that has no crystalline order whatsoever, which opens up a whole new approach to realizing topological superconductivity, in particular, one without the need to pay attention to the details of individual constituents. Ideally, regular deposition methods which are used to produce e.g. thin films could thus also be used to construct topological matter.

We found that one-dimensional impurity chains placed on the surface of a p-wave superconductor can host topological excitations at the ends of the chain, with up to 4 non-trivial topological phases. The work was published in Ref. [3]. We investigated the problem even far away from the deep-dilute regime. This was achieved by formulating the problem in terms of a non-linear eigenvalue problem, a method first employed in Ref. [22]. The topological gaps protecting the phases were found to be a significant fraction of the underlying superconducting gap, promising good robustness of the phases if the system were to be physically realized. The near-perfect localization of the MBSs to the ends of the chain may offer easy probing and

manipulation of the exotic quasiparticle excitations.

In our work on random lattices, we investigated ferromagnetic spins positioned on a lattice with the coordinates drawn from a uniform distribution. The underlying model of superconductivity is presented in Ref. [30]. We observed that our model supports one topologically non-trivial phase, which emerges seemingly only above a critical density value. As such, we presented the first-ever realistic candidate for an amorphous topological superconductor, lacking any crystalline order. This could have many potential applications in future fabrication of topological materials for use in quantum computers. The very simple and general behavior of the topology depending on the lattice density gives unprecedented flexibility for the engineering of topological phases.

Appendix A

Non-linear eigenvalue problem

In Ch. 3, we concerned ourselves with a one-dimensional chain of potential impurities placed on top of a two-dimensional p-wave superconductor. In this appendix, we present the explicit expressions left out of the main text, and derive the relevant equations, with the goal of ultimately obtaining Eq. (3.8).

Our starting point is the Bogoliubov-de Gennes (BdG) Hamiltonian

$$\mathcal{H} = \xi_{\mathbf{k}}\tau_z + \Delta(k_x\tau_x - k_y\tau_y) + U\sum_i \tau_z\delta(\mathbf{r} - \mathbf{r}_i), \tag{A.1}$$

where $\xi_{\mathbf{k}} = k^2/2m - \mu$ is the kinetic energy of the electrons, $\mu = k_F^2/2m$ is the chemical potential, and m is the effective mass of the electrons. The τ_i are Pauli matrices acting in the particle-hole space; even though we will not encounter any other such matrices in this appendix, the Pauli matrices σ_i found elsewhere in the thesis act in the spin space. Inserting this into the BdG equation $\mathcal{H}\Psi = E\Psi$, we obtain

$$\left[E - \xi_{\mathbf{k}}\tau_z - \Delta(k_x\tau_x - k_y\tau_y)\right]\Psi(\mathbf{r}) = U\sum_i \tau_z\delta(\mathbf{r} - \mathbf{r}_i)\Psi(\mathbf{r}_i) \tag{A.2}$$

Next we use the two-dimensional Fourier transform:

$$\Psi_{\mathbf{k}} = \int d\mathbf{r} e^{-i\mathbf{k}\cdot\mathbf{r}}\Psi(\mathbf{r}) \qquad \Longleftrightarrow \qquad \Psi(\mathbf{r}) = \int \frac{d\mathbf{k}}{(2\pi)^2} e^{i\mathbf{k}\cdot\mathbf{r}}\Psi_{\mathbf{k}}$$

Multiplying Eq. (A.2) by $e^{-i\mathbf{k}\cdot\mathbf{r}}$ and integrating over $d\mathbf{r}$, we get

$$\begin{aligned}\left[E-\xi_{\mathbf{k}}\tau_z-\Delta(k_x\tau_x-k_y\tau_y)\right]\Psi_{\mathbf{k}} &= U\sum_j \tau_z\int d^2r\,\delta(\mathbf{r}-\mathbf{r}_j)\Psi(\mathbf{r}_j)e^{-i\mathbf{k}\cdot\mathbf{r}}\\ &= U\sum_j e^{-i\mathbf{k}\cdot\mathbf{r}_j}\tau_z\Psi(\mathbf{r}_j)\\ \iff \qquad \Psi_{\mathbf{k}} &= U\sum_j \frac{e^{-i\mathbf{k}\cdot\mathbf{r}_j}}{E-\xi_{\mathbf{k}}\tau_z-\Delta(k_x\tau_x-k_y\tau_y)}\tau_z\Psi(\mathbf{r}_j) \quad \text{(A.3)}\end{aligned}$$

Now, going back by multiplying by $e^{i\mathbf{k}\cdot\mathbf{r}}$ and integrating over $d\mathbf{k}$ then yields

$$\Psi(\mathbf{r}) = U\int\frac{d\mathbf{k}}{(2\pi)^2}\sum_j \frac{e^{i\mathbf{k}\cdot(\mathbf{r}-\mathbf{r}_j)}}{E-\xi_{\mathbf{k}}\tau_z-\Delta(k_x\tau_x-k_y\tau_y)}\tau_z\Psi(\mathbf{r}_j). \quad \text{(A.4)}$$

Defining

$$J_E(\mathbf{r}) \equiv \frac{U}{(2\pi)^2}\int d\mathbf{k}\left[E-\xi_{\mathbf{k}}\tau_z-\Delta(k_x\tau_x-k_y\tau_y)\right]^{-1}e^{i\mathbf{k}\cdot\mathbf{r}}, \quad \text{(A.5)}$$

this becomes (evaluated at $\mathbf{r}=\mathbf{r}_i$)

$$\Psi(\mathbf{r}_i) = \sum_j J_E(\mathbf{r}_i-\mathbf{r}_j)\tau_z\Psi(\mathbf{r}_j). \quad \text{(A.6)}$$

Separating the term $j=i$ from the sum, we obtain the equation

$$\left[1-J_E(\mathbf{0})\tau_z\right]\Psi(\mathbf{r}_i) = \sum_{j\neq i} J_E(\mathbf{r}_i-\mathbf{r}_j)\tau_z\Psi(\mathbf{r}_j) \quad \text{(A.7)}$$

In anticipation of the final form of the desired matrix equation, we multiply the BdG equation (A.7) by τ_z from the left to obtain

$$\left[\tau_z-\tau_z J(\mathbf{0})\tau_z\right]\Psi(\mathbf{r}_i) = \sum_{j\neq i}\tau_z J(\mathbf{r}_i-\mathbf{r}_j)\tau_z\Psi(\mathbf{r}_j), \quad \text{(A.8)}$$

where moving in the τ_z is easy due to the properties of the Pauli matrices. Now for the evaluation of the integral $J_E(\mathbf{r})$. We first need to invert the matrix in the integrand, which is again remarkably facilitated by the anticommutativity of the Pauli matrices:

$$\begin{aligned}&\Big(E+\xi_{\mathbf{k}}\tau_z+\Delta(k_x\tau_x-k_y\tau_y)\Big)\Big(E-\xi_{\mathbf{k}}\tau_z-\Delta(k_x\tau_x-k_y\tau_y)\Big)\\ &\qquad = \left(E^2-\xi_{\mathbf{k}}^2-\Delta^2k^2\right)\mathbb{1}_{2\times2}\end{aligned}$$

and so we can write the integral in the form

$$J_E(\mathbf{r}) = U \int \frac{d\mathbf{k}}{(2\pi)^2} \frac{E + \xi_{\mathbf{k}}\tau_z + \Delta(k_x\tau_x - k_y\tau_y)}{E^2 - \xi_{\mathbf{k}}^2 - \Delta^2 k^2} e^{i\mathbf{k}\cdot\mathbf{r}} \tag{A.9}$$

We first note that the integral diverges for $\mathbf{r} = 0$. This is ultimately due to the limitations of the BCS model as a low-energy theory. As is standard in the field, we linearize k, assuming it is close to the Fermi level. This is done by expanding $\xi_{\mathbf{k}}$ to linear order in $(k-k_F)$: $\xi_{\mathbf{k}} = 0 + v_F(k-k_F) + \mathcal{O}(k-k_F)^2$, leading to $k \approx k_F + \xi_{\mathbf{k}}/v_F$. We will do this in the integrals throughout this section. For $\mathbf{r} = 0$, the terms with k_x and k_y vanish under angular integration, and the remaining terms are independent of the angle, so we obtain, after linearization,

$$J_E(\mathbf{0}) \approx U\nu_0 \int_{-\infty}^{\infty} d\xi_{\mathbf{k}} \frac{E + \xi_{\mathbf{k}}\tau_z}{E^2 - \xi_{\mathbf{k}}^2 - \Delta^2(\xi_{\mathbf{k}}/v_F + k_F)^2}, \tag{A.10}$$

where the density of states ν_0 comes from

$$\frac{dk}{d\xi_{\mathbf{k}}} = \left(\frac{dn}{dk}\right)^{-1} \frac{dn}{d\xi_{\mathbf{k}}} \approx \left(\frac{d}{dk}\frac{\pi k^2}{(2\pi)^2}\right)^{-1} \nu_0 = \frac{2\pi\nu_0}{k}. \tag{A.11}$$

This integral is readily solved by use of the residue formula, yielding

$$J_E(\mathbf{0}) \approx \frac{\alpha}{\sqrt{\beta}} \left[\tilde{\Delta}\tau_z - E\right] \tag{A.12}$$

where $\alpha = \pi\nu_0 U$, $\beta = \Delta^2 k_F^2 - \gamma E^2$ and $\tilde{\Delta} = \Delta^2 \frac{k_F}{v_F \gamma}$ with $\gamma = 1 + \frac{\Delta^2}{v_F^2}$.

For non-zero $\mathbf{r}$, there is now a non-trivial angular part sitting in the term involving Δ,

$$\int d\mathbf{k} \frac{E + \xi_{\mathbf{k}}\tau_z + \Delta(k_x\tau_x - k_y\tau_y)}{E^2 - \xi_{\mathbf{k}}^2 - \Delta^2 k^2} e^{i\mathbf{k}\cdot\mathbf{r}}. \tag{A.13}$$

We make use of the following integral representation for the Bessel functions J_0, J_1 of the first kind

$$J_0(x) = \frac{1}{2\pi}\int_0^{2\pi} dt e^{ix\cos t} \qquad J_1(x) = -J_0'(x) \tag{A.14}$$

and so using $\int d\varphi i k_j e^{i\mathbf{k}\cdot\mathbf{r}} = \partial_j \int d\varphi e^{i\mathbf{k}\cdot\mathbf{r}}$, the angular integral gives us two Bessel

functions:

$$\int d\mathbf{k}\frac{E+\xi_{\mathbf{k}}\tau_z+\Delta(k_x\tau_x-k_y\tau_y)}{E^2-\xi_{\mathbf{k}}^2-\Delta^2k^2}e^{i\mathbf{k}\cdot\mathbf{r}}= \\ 2\pi\int_0^\infty dkk\frac{(E+\xi_{\mathbf{k}}\tau_z)\,J_0(kr)+ik\frac{\Delta}{r}\,(x\tau_x-y\tau_y)\,J_1(kr)}{E^2-\xi_{\mathbf{k}}^2-\Delta^2k^2}. \tag{A.15}$$

After linearization, use of a suitable representation for the Bessel functions brings the remaining integrals into a form that can readily be solved through residue integration. Then, using the following representations for the modified Bessel and Struve functions,

$$I_0(z)-\mathbf{L}_0(z)=\frac{1}{\pi}\int_0^\pi e^{-z\sin t}dt \tag{A.16}$$

$$I_1(z)-\mathbf{L}_1(z)=\frac{2}{\pi}+\frac{i}{\pi}\int_0^\pi e^{it-z\sin t}dt, \tag{A.17}$$

we obtain

$$J_E(x\neq 0)\approx\alpha\bigg[\frac{-E}{\sqrt{\beta}}\,\mathrm{Re}\,(\Phi_0)+\Big(\frac{\tilde{\Delta}}{\sqrt{\beta}}-\frac{1}{\gamma}\,\mathrm{Im}\,(\Phi_0)\Big)\tau_z \\ -\frac{i\Delta\,\mathrm{sgn}(x)}{\gamma}\Big(\frac{1}{v_F}\Big[\frac{2}{\pi}-\mathrm{Re}\,(\Phi_1)\Big]+\frac{k_F}{\sqrt{\beta}}\,\mathrm{Im}\,(\Phi_1)\Big)\tau_x\bigg] \tag{A.18}$$

where we have set y to zero due to the one-dimensional structure of the system, as in Ch. 3. We have here defined the functions $\Phi_n\equiv I_n(x\Omega)-\mathbf{L}_n(x\Omega)$, where $\Omega=\frac{1}{\gamma}\left(\frac{\sqrt{\beta}}{v_F}+ik_F\right)$, and $I_n(x)$ and $\mathbf{L}_n(x)$ are the modified Bessel and Struve functions of the first kind, respectively.

After substituting the obtained expressions for the integrals J_E, and grouping together terms with same prefactors, we finally arrive at

$$\frac{1}{\sqrt{\beta}}\begin{pmatrix}(\varepsilon-1)A & B\\ B & (\varepsilon+1)A\end{pmatrix}\Psi=\begin{pmatrix}C-\alpha^{-1} & D\\ D & \alpha^{-1}-C\end{pmatrix}\Psi, \tag{A.19}$$

where $\varepsilon=E/\tilde{\Delta}$, $\Psi^T=[\Psi(x_1)^T\ldots\Psi(x_N)^T]$ is a $2N\times 1$ spinor. Here we have defined

the submatrices

$$A_{ij} = \tilde{\Delta}[\delta_{ij} + (1 - \delta_{ij}) \operatorname{Re} \Phi^0_{ij}] \tag{A.20}$$

$$B_{ij} = i\,(\delta_{ij} - 1)\,\gamma^{-1} \Delta k_F (\operatorname{Im} \Phi^1_{ij}) \frac{x}{r} \tag{A.21}$$

$$C_{ij} = (\delta_{ij} - 1)\,\gamma^{-1} \operatorname{Im} \Phi^0_{ij} \tag{A.22}$$

$$D_{ij} = i\,(1 - \delta_{ij})\,\frac{\tilde{\Delta}}{\Delta k_F} \left(\tfrac{2}{\pi} - \operatorname{Re} \Phi^1_{ij}\right) \frac{x}{r}. \tag{A.23}$$

Above we use the shorthand $x \equiv x_{ij} \equiv x_i - x_j$ and $r \equiv |x_{ij}|$, and $\Phi^n_{ij} \equiv \Phi_n(x_{ij})$ for the special functions. Now, A_{ij} and C_{ij} are real and symmetric under the exchange $i \leftrightarrow j$, whereas B_{ij} and D_{ij} are antisymmetric, but purely imaginary, so these are all clearly Hermitian. Thus we have now brought the non-linear eigenvalue equation into the desired form.

Appendix B

Solution to the subgap spectrum

In this appendix, we outline the steps only briefly mentioned in Sec. 3.1. As motivated in the main text, use of a periodic lattice allows us to make analytical progress by continuing the analysis in reciprocal space. We thus define the Fourier transforms of the submatrices, given by

$$a_k = \sum_j A_{ij} e^{ika(i-j)}, \tag{B.1}$$

with analogous expressions for b_k, c_k, and d_k. We could give explicit expressions for the four coefficients, but they do not simplify meaningfully, and give no further useful information, so we will stick to the defining identity (B.1). This brings us to the equation

$$\frac{1}{\sqrt{\beta}} \begin{pmatrix} (\varepsilon-1)a_k & b_k \\ b_k & (\varepsilon+1)a_k \end{pmatrix} \psi_k = \begin{pmatrix} c_k-\alpha^{-1} & d_k \\ d_k & \alpha^{-1}-c_k \end{pmatrix} \psi_k, \tag{B.2}$$

the Fourier space equivalent of Eq. (A.19). Note that this equation is valid for all N values of k; it will suffice to write it for a generic k. Now we can express our previous eigenvalue equation in a more workable form. Moving everything to the left hand side, the equation takes the form $G_k^{-1}\psi_k = 0$, where

$$G_k^{-1} = \begin{pmatrix} (\varepsilon-1)a_k - \sqrt{\beta}(c_k - \frac{1}{\alpha}) & b_k - \sqrt{\beta}d_k \\ b_k - \sqrt{\beta}d_k & (\varepsilon+1)a_k + \sqrt{\beta}(c_k - \frac{1}{\alpha}) \end{pmatrix}. \tag{B.3}$$

As with any matrix equation of this form, we seek non-trivial solutions by requiring that the matrix G^{-1} be singular; the energy bands can be solved from the condition $\det(G_k^{-1}) = 0$ for each k. Now, the energy dependence in the Fourier transformed coefficients is negligible, as discussed in Sec. 3.1. Thus we will approximate these coefficients by setting their energy arguments to zero: $a_k \to \tilde{a}_k \equiv \lim_{E\to 0} a_k$, and so on. However, we will forego the unnecessary $\tilde{a}_k$ notation, and just keep the notation as it is with no risk of confusion. There is one more thing to note about the energy dependence of the above matrix. Incidentally, expanding the determinant $\det(G^{-1})$ explicitly, we have a cancellation of terms linear in ε, and so we see that the only energy dependence outside of β is a single term $\varepsilon^2 a_k^2$, which we promptly rewrite in terms of $\beta = \Delta^2 k_F^2 - \gamma\tilde{\Delta}^2\varepsilon^2$. The condition $\det(G^{-1}) = 0$ then takes the form of a quadratic equation in $\sqrt{\beta}$:

$$P_2\beta + P_1\sqrt{\beta} + P_0 = 0, \tag{B.4}$$

with the coefficients

$$\begin{aligned} P_{0,k} &= a_k^2(1 - \gamma v_F^2/\Delta^2) + b_k^2 \\ P_{1,k} &= 2(a_k c_k' - b_k d_k) \\ P_{2,k} &= a_k^2/\gamma\tilde{\Delta}^2 + c_k'^2 + d_k^2 \end{aligned}$$

where we have defined the shorthand $c_k' = c_k - \alpha^{-1}$. The quadratic equation (B.4) is easily solved for β, but we must note that for each k there will be both a positive and a negative solution for $\sqrt{\beta}$, only one of which is sensible for a manifestly non-negative quantity. Thus the energies E can be extracted as

$$E_k = \pm\sqrt{(\Delta^2 k_F^2 - \beta_k)\gamma^{-1}}. \tag{B.5}$$

Note how the energy eigenvalues come in pairs $\pm E_k$, which is, of course, to be expected of a system equipped with PHS. This concludes our treatment of the momentum space analysis for the non-linear eigenvalue problem and the energy eigenvalues extracted from it.

Appendix C

Model of topological superconductivity

In Ch. 4, we briefly introduced a model of topological superconductivity in two dimensions involving ferromagnetic impurities. Our work on topological phases in random lattices is based on this model, and in this appendix we supply the details for it that we previously left out. The model describes a two-dimensional superconductor decorated with a 2D lattice of ferromagnetic impurities on its surface, presented in Refs. [30, 34]. For regular lattices, this model gives rise to a sea of different topological phases, and we apply it to amorphous materials, where the lattice sites are given at random.

The bulk electrons of the system in question are described by the Bogoliubov-de Gennes Hamiltonian

$$\mathcal{H}^{\text{bulk}} = \xi_{\mathbf{k}}\tau_z + \alpha_R(\boldsymbol{\sigma} \times \mathbf{k})_z\tau_z + \Delta\tau_x, \tag{C.1}$$

where $\xi_{\mathbf{k}} = k^2/2m - \mu$ is the kinetic energy of the electrons as before, and μ is the Fermi energy. α_R denotes the Rashba spin-orbit coupling strength, and Δ stands for the superconducting pairing amplitude. Similarly to the Hamiltonian used for the one-dimensional system in Ch. 3, we also have an impurity term $\mathcal{H}^{\text{imp}}$ in our

Hamiltonian, so that $\mathcal{H} = \mathcal{H}^{\text{bulk}} + \mathcal{H}^{\text{imp}}$, with

$$\mathcal{H}^{\text{imp}} = -J \sum_i \mathbf{S}_i \cdot \boldsymbol{\sigma} \delta(\mathbf{r} - \mathbf{r}_i). \tag{C.2}$$

The magnetic adatoms interact with strength J, $\mathbf{S}_i$ is the spin of the impurity on site i, and the sum runs over all impurity sites. The delta functions on each lattice site $\mathbf{r}_i$ embody the localization of the impurities to fixed sites.

We now define the dimensionless impurity strength $\alpha = \pi J S \mathcal{N}$, where $S = |\mathbf{S}_i|$ is the magnitude of the spins, and $\mathcal{N}$ is the spin-averaged density of states. We also make the simplifying assumption that $\alpha \approx 1$, which means that the energy of the individual Shiba states $\varepsilon_0 = \Delta(1 - \alpha)$ lies close to zero, i.e. close to the center of the superconducting gap. Moreover, we assume that the lattice constant a for the impurities is large enough, $k_F a \gg 1$, so that the impurity band is well within the gap. In this deep-dilute limit, we can now obtain an effective low-energy tight-binding Hamiltonian. This is done by similar analysis of the Hamiltonian (C.1), (C.2) as done in Ch. 3, but also expanding the relevant equations to linear order in E, that is, in $(1 - \alpha)$. The resulting Hamiltonian is given by

$$H_{mn} = \begin{pmatrix} h_{mn} & \Delta_{mn} \\ (\Delta_{mn})^\dagger & -h^*_{mn} \end{pmatrix}, \tag{C.3}$$

where h_{mn} and Δ_{mn} are $N \times N$ blocks, whose expressions are given by

$$h_{mn} = \begin{cases} \varepsilon_0, & m = n \\ \dfrac{\Delta}{2}[I_1^-(r_{mn}) + I_1^+(r_{mn})]\langle \uparrow_m | \uparrow_n \rangle & \\ \quad + i\dfrac{\Delta}{2}[I_3^-(r_{mn}) - I_3^+(r_{mn})] \left[\langle \uparrow_m | \sigma_x | \uparrow_n \rangle \dfrac{y_{mn}}{r_{mn}} - \langle \uparrow_m | \sigma_y | \uparrow_n \rangle \dfrac{x_{mn}}{r_{mn}} \right], & m \neq n \end{cases} \tag{C.4}$$

and

$$\Delta_{mn} = \begin{cases} 0, & m = n \\ -\dfrac{\Delta}{2}[I_2^-(r_{mn}) + I_2^+(r_{mn})]\langle \uparrow_m | \downarrow_n \rangle & \\ \quad - i\dfrac{\Delta}{2}[I_4^-(r_{mn}) - I_4^+(r_{mn})] \left[\langle \uparrow_m | \sigma_x | \downarrow_n \rangle \dfrac{y_{mn}}{r_{mn}} - \langle \uparrow_m | \sigma_y | \downarrow_n \rangle \dfrac{x_{mn}}{r_{mn}} \right], & m \neq n \end{cases} \tag{C.5}$$

Above, $\mathbf{r}_m = (x_m, y_m)$, $r_{mn} = |\mathbf{r}_m - \mathbf{r}_n|$ is the distance between two lattice sites m and n, and likewise $x_{mn} = x_m - x_n$ and $y_{mn} = y_m - y_n$ are the corresponding

coordinate differences. Also, $|\uparrow_n\rangle$, $|\downarrow_n\rangle$ denote eigenstates of the magnetic moments, $\mathbf{S}_m \cdot \boldsymbol{\sigma}|\uparrow_n\rangle = +|\mathbf{S}_m||\uparrow_n\rangle$, and likewise for $|\downarrow_n\rangle$ with the opposite sign, and ε_0 is the onsite energy, which comes from the decoupled impurity energy. The functions $I_n^{\pm}$ appearing in the expressions for h_{mn}, Δ_{mn} are defined by use of

$$\hat{I}_1^{\pm}(r) = -\operatorname{Re}\left[J_0(\zeta^{\pm}r) + iH_0(\zeta^{\pm}r)\right] \tag{C.6}$$

$$\hat{I}_2^{\pm}(r) = \quad \operatorname{Im}\left[J_0(\zeta^{\pm}r) + iH_0(\zeta^{\pm}r)\right] \tag{C.7}$$

$$\hat{I}_3^{\pm}(r) = \quad \operatorname{Im}\left[iJ_1(\zeta^{\pm}r) + H_{-1}(\zeta^{\pm}r)\right] \tag{C.8}$$

$$\hat{I}_4^{\pm}(r) = \quad \operatorname{Re}\left[iJ_1(\zeta^{\pm}r) + H_{-1}(\zeta^{\pm}r)\right] \tag{C.9}$$

where $\zeta^{\pm} = k_F^{\pm} + i/\xi$, the $k_F^{\pm}$ are Fermi wave numbers altered due to SOC, $k_F^{\pm} = (\sqrt{1+\lambda^2} \mp \lambda)k_F$, where $\lambda = \alpha_R/v_F$ is the dimensionless Rashba coupling. The $I_n^{\pm}$ are related to these auxiliary functions through $I_n^{\pm} = (1 \mp \lambda/\sqrt{1+\lambda^2})\hat{I}_n^{\pm}$.

We should also mention that in the case of ferromagnetic spins, the spin vectors $\mathbf{S}_i$ all point in the same direction, say, $\mathbf{S}_i = S\hat{\mathbf{e}}_z$. This leads to most of the brackets such as $\langle\uparrow_m \mid \downarrow_n\rangle$ appearing in expressions (C.4), (C.5) to vanish, and we are left with a simpler Hamiltonian, consisting of the submatrices

$$h_{mn} = \begin{cases} \varepsilon_0, & m = n \\ \frac{\Delta}{2}\left[I_1^-(r_{mn}) + I_1^+(r_{mn})\right], & m = n \end{cases}, \tag{C.10}$$

$$\Delta_{mn} = \begin{cases} 0, & m = n \\ \frac{\Delta}{2}\left[I_4^-(r_{mn}) - I_4^+(r_{mn})\right]\frac{x_{mn}-iy_{mn}}{r_{mn}}, & m = n \end{cases}. \tag{C.11}$$

These are only valid in the case of spins pointing in exactly in the same direction. Even for spins only nearly polarized in the same direction, these equations become approximations, and one is forced to use Eqs. (C.4), (C.5) for a more precise analysis.

References

1 M. Ezawa, Y. Tanaka, and N. Nagaosa, Sci. Rep. **3**, 2790 (2013).

2 A. Agarwala and V. B. Shenoy, Phys. Rev. Lett. **118**, 236402 (2017).

3 I. Sahlberg, A. Weststrom, K. Pöyhönen, and T. Ojanen, Phys. Rev. B **95**, 184512 (2017).

4 K. Pöyhönen, I. Sahlberg, A. Weststrom, and T. Ojanen, arXiv:1712.07486 (2017).

5 P. W. Anderson, Science **177**, 4047 (1972).

6 J. K. Pachos, *Introduction To Topological Quantum Computation* (Cambridge University Press, 2012).

7 J. Alicea, Y. Oreg, G. Refael, F. von Oppen, and M. P. A. Fisher, Nat. Phys. **7**, 412 (2011).

8 T. Hyart, B. van Heck, I. C. Fulga, M. Burrello, A. R. Akhmerov, and C. W. J. Beenakker, Phys. Rev. B **88**, 035121 (2013).

9 R. P. Feynman, Int. J. Theor. Phys **21**, 467 (1982).

10 S. Boixo, T. F. Rønnow, S. V. Isakov, Z. Wang, D. Wecker, D. A. Lidar, J. M. Martinis, and M. Troyer, Nat. Phys. **10**, 218 (2014).

11 S. Das Sarma, M. Freedman, and C. Nayak, Phys. Rev. Lett. **94**, 166802 (2005).

12 C. Nayak, S. H. Simon, A. Stern, M. Freedman, and S. Das Sarma, Rev. Mod. Phys. **80**, 1083 (2008).

13 H. Kamerlingh Onnes, Comm. Phys. Lab. Univ. Leiden, 122b (1911).

14 W. Meissner and R. Ochsenfeld, Die Naturwissenschaften **21**, 44 (1933).

15 M. Tinkham, *Introduction to Superconductivity: Second Edition* (Dover Publications, 2004).

16 A. P. Drozdov, M. I. Eremets, I. A. Troyan, V. Ksenofontov, and S. I. Shylin, Nature **525**, 73 (2015).

17 J. Bardeen, L. N. Cooper, and J. R. Schrieffer, Phys. Rev. **106**, 162 (1957).

18 J. Bardeen, L. N. Cooper, and J. R. Schrieffer, Phys. Rev. **108**, 1175 (1957).

19 H. Bruus and K. Flensberg, *Many-body Quantum Theory in Condensed Matter Physics: An Introduction* (Oxford University Press, 2004).

20 A. Y. Kitaev, Phys. Usp. **44**, 131 (2001).

21 B. A. Bernevig and T. L. Hughes, *Topological insulators and topological superconductors* (Princeton University Press, 2013).

22 A. Weststrom, K. Pöyhönen, and T. Ojanen, Phys. Rev. B **91**, 064502 (2015).

23 A. Weststrom, K. Pöyhönen, and T. Ojanen, Phys. Rev. B **94**, 104519 (2016).

24 K. Pöyhönen, A. Weststrom, and T. Ojanen, Phys. Rev. B **93**, 014517 (2016).

25 S. Ryu, A. P. Schnyder, A. Furusaki, and A. W. W. Ludwig, New J. Phys. **12**, 065010 (2010).

26 A. P. Schnyder, S. Ryu, A. Furusaki, and A. W. W. Ludwig, Phys. Rev. B **78**, 195125 (2008).

27 G. E. Volovik, *The Universe in a Helium Droplet* (Oxford University Press, 2003).

28 C. Kallin and A. J. Berlinsky, J. Phys. Condens. Matter **21**, 164210 (2009).

29 K. Kobayashi, T. Ohtsuki, and K.-I. Imura, Phys. Rev. Lett. **110**, 236803 (2013).

30 J. Röntynen and T. Ojanen, Phys. Rev. B **93**, 094521 (2016).

31 T. A. Loring and M. B. Hastings, EPL **92**, 67004 (2010).

32 D. Toniolo, arXiv:1708.05912 (2017).

33 G. R. Grimmett, *Percolation* (Springer, 1999).

34 J. Röntynen and T. Ojanen, Phys. Rev. Lett. **114**, 236803 (2015).